Inorganic Chemistry

Article

pubs.acs.org/IC

C−C Bond Formation and Related Reactions at the CNC Backbone in (smif)FeX (smif = 1,3-Di-(2-pyridyl)-2-azaallyl): Dimerizations, 3 + 2 Cyclization, and Nucleophilic Attack; Transfer Hydrogenations and Alkyne Trimerization (X = $N(TMS)_2$, dpma = (Di-(2-pyridyl-methyl)-amide))

Brenda A. Frazier,[†] Valerie A. Williams,[†] Peter T. Wolczanski,*[,†] Suzanne C. Bart,[‡,∥] Karsten Meyer,[‡] Thomas R. Cundari,[§] and Emil B. Lobkovsky[†]

[†]Department of Chemistry & Chemical Biology, Baker Laboratory, Cornell University, Ithaca, New York 14853, United States

[‡]Department of Chemistry & Pharmacy, University of Erlangen-Nuremberg, Egerlandstr. 1·D-91058 Erlangen, Germany

[§]Department of Chemistry, Center for Advanced Scientific Computing and Modeling (CASCaM), University of North Texas, Box 305070, Denton, Texas 76203-5070, United States

Supporting Information

ABSTRACT: Molecular orbital analysis depicts the CNC^{nb} backbone of the smif (1,3-di-(2-pyridyl)-2-azaallyl) ligand as having singlet diradical and/or ionic character where electrophilic or nucleophilic attack is plausible. Reversible dimerization of (smif)Fe{$N(SiMe_3)_2$} (**1**) to [{$(Me_3Si)_2N$}Fe]$_2$(μ-κ^3,κ^3-*N*,py$_2$-smif,smif) (**2**) may be construed as diradical coupling. A proton transfer within the backbone-methylated, and *o*-pyridine-methylated smif of putative (^{b}Me$_2$^{o}Me$_2$smif)Fe-$N(SiMe_3)_2$ (**8**) provides a route to [{$(Me_3Si)_2N$}Fe]$_2$(μ-κ^4,κ^4-*N*,py$_2$,C-(^{b}Me,^{b}CH$_2$,^{o}Me$_2$(smif)H))$_2$ (**9**). A 3 + 2 cyclization of ditolyl-acetylene occurs with **1**, leading to the dimer [{2,5-di(pyridin-2-yl)-3,4-di-(*p*-tolyl-2,5-dihydropyrrol-1-ide)}FeN-$(SiMe_3)_2$]$_2$ (**11**), and the collateral discovery of alkyne cyclotrimerization led to a brief study that identified Fe$(N(SiMe_3)_2)_2$(THF) as an effective catalyst. Nucleophilic attack by (smif)$_2$Fe (**13**) on ^{t}BuNCO and (2,6-^{i}Pr$_2$C$_6$H$_3$)NCO afforded (RNHCO-smif)$_2$Fe (**14a**, R = ^{t}Bu; **14b**, 2,6-^{i}PrC$_6$H$_3$). Calculations suggested that (dpma)$_2$Fe (**15**) would favorably lose dihydrogen to afford (smif)$_2$Fe (**13**). H_2-transfer to alkynes, olefins, imines, PhN═NPh, and ketones was explored, but only stoichiometric reactions were affected. Some physical properties of the compounds were examined, and X-ray structural studies on several dinuclear species were conducted.

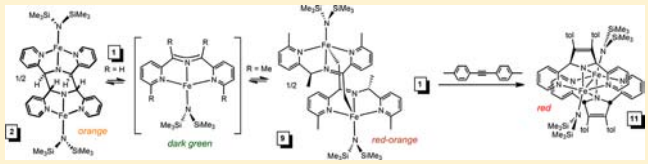

1. INTRODUCTION

While examining polydentate chelates of first-row transition elements,[1−3] a decomposition led to the synthesis of (smif)-$CrN(TMS)_2$ (smif = 1,3-di-(2-pyridyl)-2-azaallyl).[1] Discovery of the anionic azaallyl anion ligand prompted the synthesis of a set of new Werner complexes, (smif)$_2$M^n (n = 0, M = V, Cr, Mn, Fe, Co, Ni, Ru; n = +1, M = Cr, Mn, Co, Rh, Ir).[4,5] The electronic properties of these complexes were investigated in response to their unusual optical densities, which are derived from intraligand (IL) transitions wherein charge is transferred from the backbone CNC^{nb} orbitals to those with pyridine π*-character.[1,4,5]

An abbreviated look at the CNC^{nb} orbital in the smif backbone, where modest contributions from the pyridine rings are ignored, is given in Figure 1.[5−7] A decomposition of the crude wavefunction renders two orbital components that are distinct: an ionic part that suggests the potential for nucleophilic/electrophilic activation of the backbone, and a covalent part that possesses singlet diradical character. Either component could direct C−C bond formation at the CNC backbone of the smif ligand,[4,7,8] such as a dimerization process.

Examples of C−C bond formation derived from backbone coupling reactions have been seen in attempts to synthesize (smif)$_2$Ti.[7] As Figure 2 reveals, (smif){Li(smif-smif)}Ti (**Ti-1**) degraded at room temperature to afford a mixture of diamagnetic products. Spectroscopic analysis (K-edge XAS, 2D NMR) of **Ti-1** and its degradation products suggested that they are best described as d^1 Ti(III) centers AF-coupled to ligand radicals: (smif){Li(smif-smif)$^{2-}$}Ti^{III} (**Ti-1**), [(smif^{2-})-Ti^{III}]$_2$(μ-κ^3,κ^3-*N*,py$_2$-smif,smif) (**Ti-2**), [(smif^{2-})Ti^{III}](κ^3-*N*,*N*(py)$_2$-smif,(smif)H) (**Ti-3**), and (smif^{2-})Ti^{III}(dmpa) (**Ti-4**). While it is likely that a bound Li(smif) unit succumbed to a nucleophilic attack of a bound smif to generate the new C−C bond in **Ti-1**, the C−C bonds in **Ti-2** can be construed as arising from nucleophilic/electrophilic attack or the coupling of diradicals; the same is true for **Ti-3**, because it is likely to be a

Received: December 19, 2012
Published: February 28, 2013

   dx.doi.org/10.1021/ic302783y | *Inorg. Chem.* 2013, 52, 3295−3312

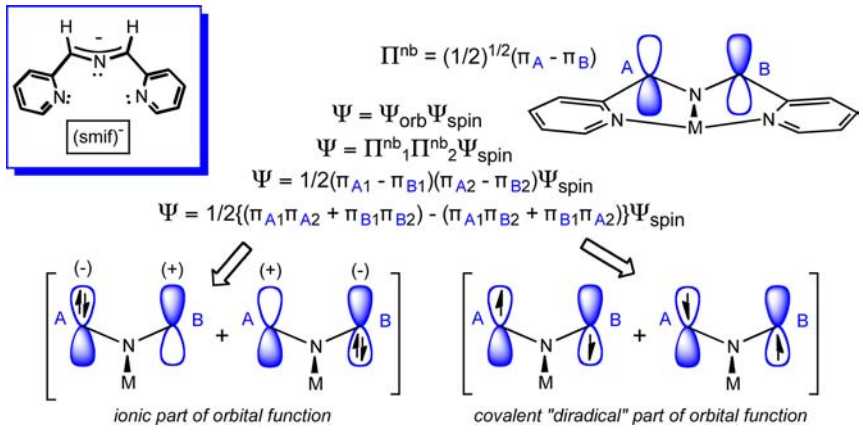

Figure 1. Expansion of a truncated smif CNC^{nb} orbital showing ionic and covalent diradical components.

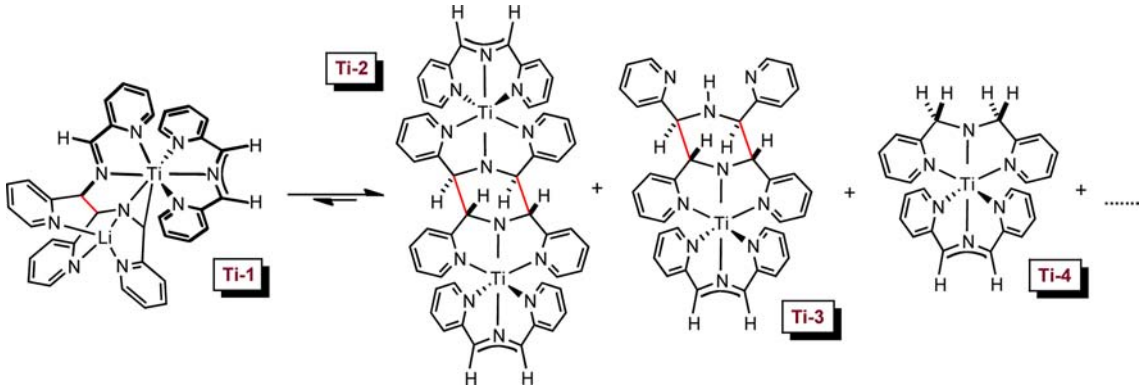

Figure 2. Various smif-containing complexes where C−C (red) or C−H bond formation has occurred via the CNC backbone of smif.

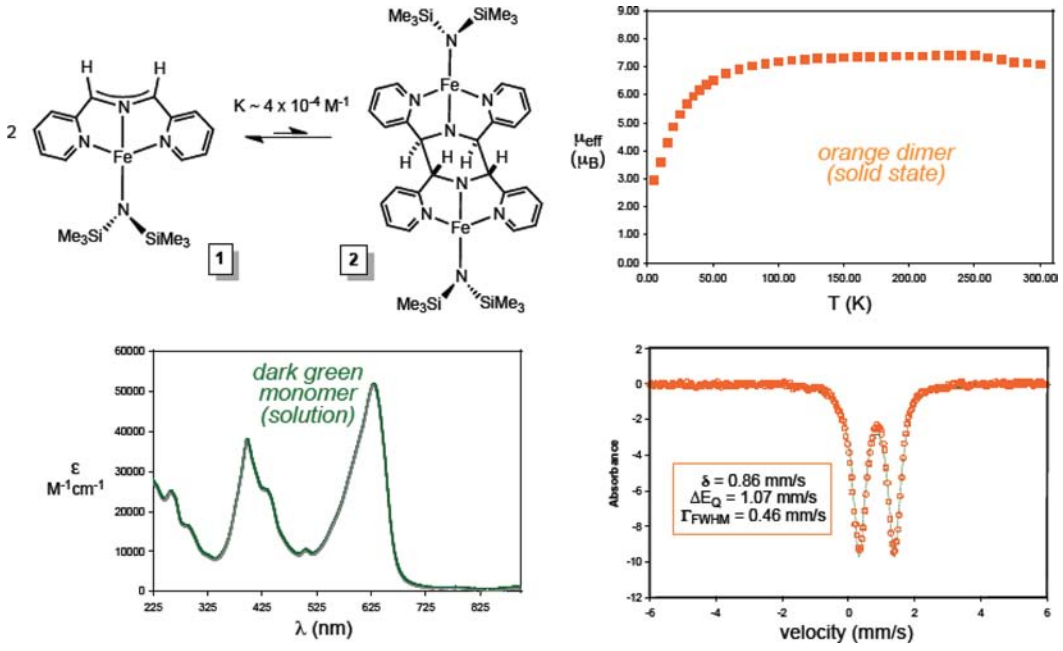

Figure 3. Green (smif)Fe{N(SiMe$_3$)$_2$} (**1**) is monomeric in solution, but in the solid state, it is a dimer, [{(Me$_3$Si)$_2$N}Fe]$_2$(μ-κ^3,κ^3-*N*,py$_2$-smif,smif) (**2**, X-ray). A μ_{eff} vs *T* (K) plot and a Mössbauer spectrum of **2** are shown.

protonolysis product derived from **Ti-2**. Redox noninnocence was previous observed in (smif)$_2$Cr, that is, (smif)(smif^{2-})-Cr^{III},[5,6] but whether such electronic factors are important to the C−C bond forming events is unclear.

Reversible carbon−carbon bond formations are often seen accompanying redox events, and such systems have been explored in the context of energy storage.[9−20] It is important to note that the transformations described herein are not triggered by external redox events, nor are the majority coupled to redox

dx.doi.org/10.1021/ic302783y | *Inorg. Chem.* 2013, 52, 3295−3312

changes at the metal. The chemistry is intrinsic to the nature of the frontier orbitals of the smif ligand. Herein are described efforts to control the smif backbone reactivity: generating carbon−carbon and carbon−hydrogen bonds at the CNC positions, and examining the means to prevent such reactivity. The first example of C−C bond formation at the backbone of smif was the case of $[\{(Me_3Si)_2N\}Fe]_2(\mu\text{-}\kappa^3,\kappa^3\text{-}N,py_2\text{-}smif,smif)$ (**2**) illustrated in Figure 3, which was briefly mentioned in a communication.[4] The examination of smif reactivity starts with this case.

2. RESULTS

2.1. Smif Backbone C−C Coupling. *2.1.1. Synthesis of* $[\{(Me_3Si)_2N\}Fe]_2(\mu\text{-}\kappa^3,\kappa^3\text{-}N,py_2\text{-}smif,smif)$ *(**2**).* The generation of $[\{(Me_3Si)_2N\}Fe]_2(\mu\text{-}\kappa^3,\kappa^3\text{-}N,py_2\text{-}smif,smif)$ (**2**) was achieved via the addition of 1,3-di-(2-pyridyl)-2-azapropene (i.e., (smif)-H)[5] to $Fe\{N(SiMe_3)_2\}_2THF$[21] in Et_2O over the course of 3 h (eq 1). From an emerald green solution distinctive for the

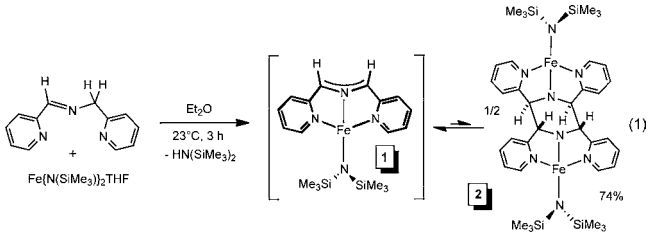

monomer (smif)$Fe\{N(SiMe_3)_2\}$ (**1**), orange crystals were isolated in 74% yield. The UV−vis spectrum of **1** manifests intense absorptions at 625 nm (ε = 52 000 M^{-1} cm^{-1}) and 398 nm (ε = 38 000 M^{-1} cm^{-1}), which constitute the "red' and "blue" intraligand transitions common to the complexes containing smif.[1,5] In contrast to its dark emerald green solutions, crystals that precipitated were orange, and lacked substantial intensity. An NMR spectral analysis[22] afforded an equilibrium constant for 2 **1** ⇄ **2** of $K_{297} \sim 4 \times 10^{-4}$, showing that the amount of C,C-coupled dimer **2** was relatively insignificant in typical solutions, with $\Delta G^\circ_{297} \sim 5$ kcal/mol.

SQUID magnetometry on **2** provided a μ_{eff} of ~6.9 μ_B at 300 K, which is essentially the value predicted for a two S = 2 centers on one molecule that do not couple. There is a substantial downturn of the μ_{eff} below 75 K as the effects of zero field splitting (ZFS) are observed. Contributions from antiferromagnetic coupling cannot be ruled out, but the d(Fe···Fe) of 6.158(2) Å renders this factor unlikely. Mössbauer spectroscopy on **2** provided parameters consistent with a low-symmetry high-spin iron(II) center.[23,24] The isomer shift is 0.86 mm/s, typical for a high-spin ferrous species, and the quadrupole splitting of 1.07 mm/s suggests significant asymmetry in the electric field, as expected for a pseudo-square-planar geometry.

2.1.2. Structure of $[\{(Me_3Si)_2N\}Fe]_2(\mu\text{-}\kappa^3,\kappa^3\text{-}N,py_2\text{-}smif,smif)$ *(**2**).* A molecular view of $[\{(Me_3Si)_2N\}Fe]_2(\mu\text{-}\kappa^3,\kappa^3\text{-}N,py_2\text{-}smif,smif)$ (**2**) is provided in Figure 4, which reveals the approximate C_{2h} symmetry of the dimer and provides selected information regarding interatomic distances and angles. Limited data collection and refinement parameters are listed in Table 1. Two pseudo-square-planar (Σ(NFeN angles) = 360.0°) iron centers are coupled via rather long carbon−carbon bonds (1.578(2) Å) connecting the two smif backbones, perhaps suggestive of the reversible monomer/dimer equilibrium. These linkages are pyramidal at the carbon, with the sum of the angles about the C6 and C7 centers averaging 110.0(24)° and 110.0(27)°, respectively. The iron−pyridine distances are long (2.1950(11), 2.1910(11) Å) in comparison to the iron backbone−amide (1.9432(10) Å) and iron−bis-trimethylsilylamide (1.9538(10) Å) bond lengths, and long relative to those

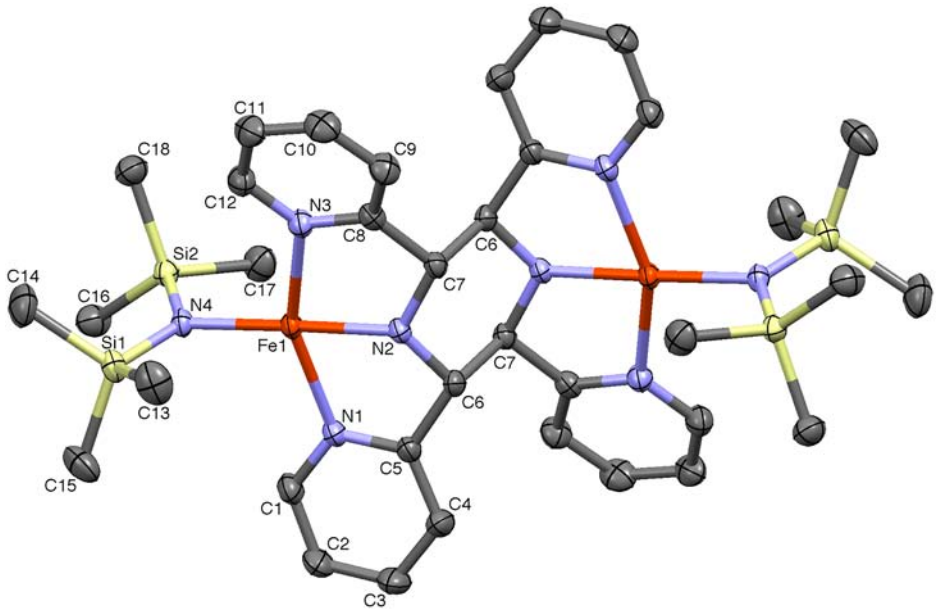

Figure 4. Molecular view of $[\{(Me_3Si)_2N\}Fe]_2(\mu\text{-}\kappa^3,\kappa^3\text{-}N,py_2\text{-}smif,smif)$ (**2**). Selected interatomic distances (Å) and angles (deg): Fe−Fe, 6.158(2); Fe−N1, 2.1950(11); Fe−N2, 1.9432(10); Fe−N3, 2.1910(11); Fe−N4, 1.9538(10); N2−C7, 1.4356(16); N2−C6, 1.4334(17); C7−C8, 1.4964(18); C5−C6, 1.5023(17); C6−C7′, 1.5781(18); N4−Si1, 1.6983(11); N4−Si2, 1.6966(11); N1−Fe−N2, 77.20(4); N1−Fe−N3, 154.48(4); N1−Fe−N4, 101.94(4); N2−Fe−N3, 77.38(4); N2−Fe−N4, 178.53(4); N3−Fe−N4, 103.43(4); Fe−N2−C6, 120.95(8); Fe−N2−C7, 120.66(8); C6−Fe−C7, 113.94(10; N2−C6−C5, 108.09(10); N2−C6−C7, 109.08(10); N2−C7−C6, 108.93(10); N2−C7−C8, 108.03(10); C5−C6−C7′, 112.72(10); C6′−C7-C8, 113.10(11).

dx.doi.org/10.1021/ic302783y | Inorg. Chem. 2013, 52, 3295−3312

Table 1. Selected Crystallographic and Refinement Data for $[\{(Me_3Si)_2N\}Fe]_2(\mu\text{-}\kappa^3,\kappa^3\text{-}N,py_2\text{-}smif,smif)$ (2), $[\{(Me_3Si)_2N\}Fe]_2(\mu\text{:}\kappa^3\text{-}N,py,py',\kappa^3\text{-}N',py'\text{,py-}^o Me_2smif\text{-}^o Me_2smif)$ (6), $[\{(Me_3Si)_2N\}Fe]_2(\mu\text{-}\kappa^4,\kappa^4\text{-}N,py_2,C\text{-}(^b Me,^b CH_2,^o Me_2(smif)H))_2$ (9), $[\{2,5\text{-Di(pyrindin-2-yl)-3,4-di-(}p\text{-tolyl-2,5-dihydropyrrol-1-ide)}\}FeN(SiMe_3)_2]_2$ (11), $(2,6\text{-}^i PrC_6H_3\text{-NHCO-smif})_2Fe$ (14b), and $(dpma)_2Fe$ (15)

	2[a]	6[a]	9[a]	11	14b[b]	15
formula	$C_{36}H_{56}N_8Si_4Fe_2$	$C_{40}H_{64}N_8Si_4Fe_2$	$C_{44}H_{72}N_8Si_4Fe_2$	$C_{68}H_{84}N_8Si_4Fe_2$	$C_{54}H_{62}N_8O_3Fe$	$C_{24}H_{24}N_6Fe$
formula wt	824.94	881.05	937.16	1237.49	926.97	452.34
space group	$P\bar{1}$	$P2_1/c$	$P\bar{1}$	$P2_1/c$	$Pcca$	$P2_12_12_1$
Z	1	2	1	4	8	8
a, Å	8.0558(5)	9.1297(5)	8.5974(6)	13.8897(7)	34.168(5)	8.5577(4)
b, Å	10.8367(7)	18.5891(9)	12.1386(9)	35.0779(17)	17.174(3)	16.6991(6)
c, Å	14.3114(9)	14.2734(9)	12.5960(9)	15.5291(8)	18.038(3)	30.5536(12)
α, deg	72.491(3)	90	87.456(5)	90	90	90
β, deg	85.244(4)	104.629(3)	81.005(5)	90.361(2)	90	90
γ, deg	81.614(4)	90	69.286(4)	90	90	90
V, Å^3	1177.73(13)	2343.8(2)	1214.34(15)	7566.0(7)	10585(3)	4366.3(3)
ρ_{calc}, g·cm^{-3}	1.163	1.248	1.282	1.086	1.163	1.376
μ, mm^{-1}	0.749	0.757	0.735	0.487	0.333	0.714
temp, K	173(2)	173(2)	173(2)	173(2)	173(2)	173(2)
λ (Å)	0.71073	0.71073	0.71073	0.71073	0.71073	0.71073
R indices	R_1 = 0.0389	R_1 = 0.0366	R_1 = 0.0384	R_1 = 0.0431	R_1 = 0.0631	R_1 = 0.0388
$[I > 2\sigma(I)]^{b,c}$	wR_2 = 0.0963	wR_2 = 0.0917	wR_2 = 0.0794	wR_2 = 0.1050	wR_2 = 0.1469	wR_2 = 0.0708
R indices	R_1 = 0.0533	R_1 = 0.0508	R_1 = 0.0586	R_1 = 0.0740	R_1 = 0.1284	R_1 = 0.0560
(all data)^{b,c}	wR_2 = 0.1018	wR_2 = 0.0991	wR_2 = 0.0858	wR_2 = 0.1141	wR_2 = 0.1702	wR_2 = 0.0769
GOF[d]	1.048	1.034	1.014	1.016	0.925	1.035

[a]One-half of the molecule is the asymmetric unit. [b]One molecule of THF per asymmetric unit. $R_1 = \sum||F_o| - |F_c||/\sum|F_o|$. [c]$wR_2 = [\sum w(|F_o| - |F_c|)^2/\sum wF_o^2]^{1/2}$. [d]GOF (all data) $= [\sum w(|F_o| - |F_c|)^2/(n-p)]^{1/2}$; n = number of independent reflections, p = number of parameters.

in $(smif)_2Fe$ (1.9634(12) Å (ave)). The bite angle of the dipyridyl-amide chelate (N1−Fe−N2, 77.20(4)°; N2−Fe−N3, 77.38(4)°; N1−Fe−N3, 154.48(4)°) is typical, and the remaining core angles (N1−Fe−N4, 101.94(4)°; N2−Fe−N4, 178.53(4)°; N3−Fe−N4, 103.43(4)°) are commensurate with the nearly planar iron center.

2.1.3. (dpma)Fe{N(SiMe$_3$)$_2$} (3) as a Model for 2. To check whether the spectral parameters and magnetic information regarding $[\{(Me_3Si)_2N\}Fe]_2(\mu\text{-}\kappa^3,\kappa^3\text{-}N,py_2\text{-smif,smif})$ (**2**) were consistent with the dimeric formulation, the di-2-pyridyl-methyl-amide (dpma) ligand[25] was examined as an analogue with a saturated backbone. The reaction of (dpma)H to $Fe\{N(SiMe_3)_2\}_2THF$ in Et_2O over the course of 12 h at 23 °C (eq 2) led to a red solution from which red crystals of

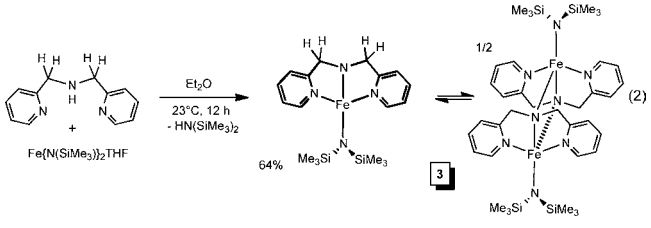

(dpma)Fe{N(SiMe$_3$)$_2$} (**3**) were obtained in 64% yield. The solubility properties of **3** and its ^{1}H NMR spectrum, which revealed C_{2v} symmetry, were consistent with a momomeric formulation, and its UV−vis spectrum was essentially featureless except for a modest maximum at 549 nm (ε = 1500 M^{-1} cm^{-1}). Contemporaneous with this work, Westerhausen et al. have prepared (dpma)Fe{N(SiMe$_3$)$_2$} (**3**) by an analogous route, and have shown it to be a dimer, that is, $[\{(Me_3Si)_2N\}Fe(\mu\text{-N,}\kappa^3\text{-}N,py_2\text{-dpma})]_2$ (**3**), in the solid state, with a μ_{eff} = 7.5 μ_B (Gouy balance).[26] For further discussion of the magnetism of **3**, see the Supporting Information.

2.1.4. Pyridine-Substituted smif Derivatives, (smif′)Fe{N(SiMe$_3$)$_2$}. To probe whether subtle electronic or steric effects would impact the solid-state dimerization characteristic of **1** to **2**, small-scale syntheses were conducted on variants of smif. The addition of 1,3-(2-pyridyl,6-methyl-2-pyridyl)-2-azapropene (i.e., (^{o}Mesmif)H)[5] to $Fe\{N(SiMe_3)_2\}_2THF$[21] in Et_2O resulted in a deep teal-green solution from which yellow-orange crystals of $[\{(Me_3Si)_2N\}Fe]_2(\mu\text{-}\kappa^3,\kappa^3\text{-}N,py_2\text{-}^o Mesmif,^o Mesmif)$ (**5**) were isolated in 47% yield (eq 3). ^{1}H NMR spectral studies

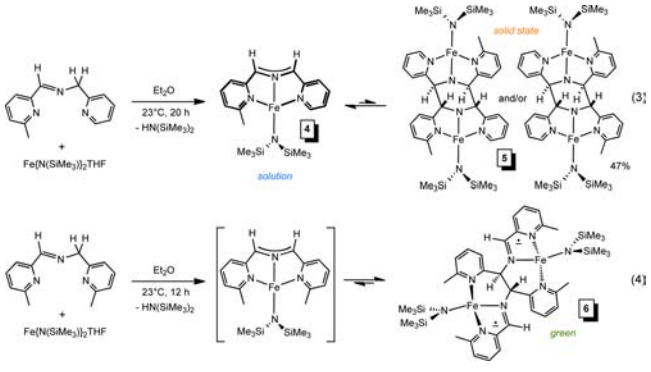

revealed a one ^{o}Mesimif and one $SiMe_3$ environment, consistent with (^{o}Mesmif)FeN(SiMe$_3$)$_2$ (**4**), which is likely to be teal-colored.[5] Given the related color changes to those in eq 1, the solid-state structure is probably dimeric; whether the expected two isomers exist as shown could not be discerned by the NMR data.

Di-*ortho*-methylation of the smif ligand proved to change the nature of the carbon−carbon bond-forming process, as shown in eq 4. Treatment of $Fe\{N(SiMe_3)_2\}_2THF$ with (^{o}Me$_2$smif)H[5] provided another dark teal solution, but a dark green microcrystalline material was eventually isolated in 33% yield.

dx.doi.org/10.1021/ic302783y | Inorg. Chem. 2013, 52, 3295−3312

The complex proved to be unstable in both solution and the solid state, and disproportionated to afford the known (^{o}Me$_2$smif)$_2$Fe, which has bands at ~580 nm (ε = 58 000 M^{-1} cm^{-1}) and ~400 nm (ε = 32 000 M^{-1} cm^{-1}) that dominate the UV−vis spectrum.[5] The intensity of these absorptions masked the true color of the major product, [{(Me$_3$Si)$_2$N}Fe]$_2$(μ:κ^3-*N*,py,py′,κ^3-*N*′,py′,-py-^{o}Me$_2$smif-^{o}Me$_2$smif) (**6**), and hampered spectral analysis. Initially fooled by the omnipresence of teal/gold (^{o}Me$_2$smif)$_2$-Fe, careful crystallization afforded pure **6**, and its structure was ascertained by X-ray crystallography.

Redox noninnocence plays a role in the carbon−carbon bond formation, as the reductive coupling of the smifs in putative (^{o}Me$_2$smif)FeN(TMS)$_2$ affords a formal Fe(I) center that reduces the pyridine-imine fragments to render the centers Fe(II). SQUID magnetometry was originally conducted on a sample, but the thermal sensitivity of **6**, and plausible contamination from S = 2 (^{o}Me$_2$smif)$_2$Fe, rendered its interpretation suspect. There are actually four spins to consider: two Fe(II) centers that are likely to be S = 2, and two pyridine-imine radicals each S = 1/2. Given the likelihood of strong AF coupling between each pyridine-imine radical and its adjacent iron(II) center, it is likely that the molecule consists of two S = 3/2 centers

*2.1.5. Structure of [{(Me$_3$Si)$_2$N}Fe]$_2$(μ:κ^3-N,py,py′,κ^3-N′,py′,-py-^{o}Me$_2$smif-^{o}Me$_2$smif) (**6**).* A molecular view of [{(Me$_3$Si)$_2$-N}Fe]$_2$(μ:κ^3-*N*,py,py′,κ^3-*N*′,py′,py-^{o}Me$_2$smif-^{o}Me$_2$smif) (**6**) is presented in Figure 5, whose caption includes selected metric parameters. Some details of the data collection and refinement can be found in Table 1. Two distorted tetrahedral N$_4$Fe centers (core angles range from 79.19(6) to 129.78(6)°) are centrosymmetric with respect to the center of the new carbon−carbon bond (d(C8−C8) = 1.561(2) Å); hence, each iron is coordinated by two *o*-Me-pyridine groups, an imine, and the (TMS)$_2$N unit. A formal oxidation state based on this coordination sphere would be Fe(I) as a consquence of the reductive coupling of the two smif units, each of which now spans two iron centers. Upon closer inspection, the pyridine-imine unit displays the telltale bond distances of a monoreduced entitly, with the imine CN elongated to 1.328(2) Å, C6−C7 shortened to 1.405(3) Å, and the pyridine CN stretched to 1.381(2) Å.[27−33] The iron centers are each ferrous, with two additional spins affiliated with the pyridine-imines. The Fe−N3 distance of 2.1464(15) Å is slightly longer than the iron−pyridine (2.0965(15) Å) and iron−imine (2.0069(15) Å) nitrogen distances within the monoreduced fragment, while the bis-TMS−amide is the shortest at 1.9489(15) Å.

2.1.6. Backbone-Substituted smif Derivatives, (smif″)Fe{N-(SiMe$_3$)$_2$}. Methylation of the CNC backbone of (smif)H and (^{o}Me$_2$smif)H was accomplished in a one-pot procedure involving sequential deprotonation and methylation events, the former via NaH, and the latter using MeI (eq 5). The methylations were nearly quantitative, such that the crude products (^{b}Me$_2$smif)H and (^{b}Me$_2$^{o}Me$_2$smif)H were used in subsequent reactions.

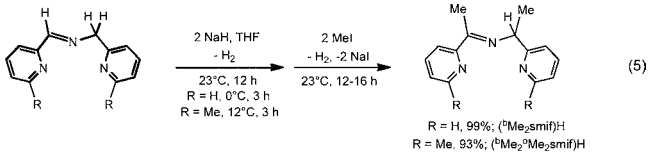

(5)

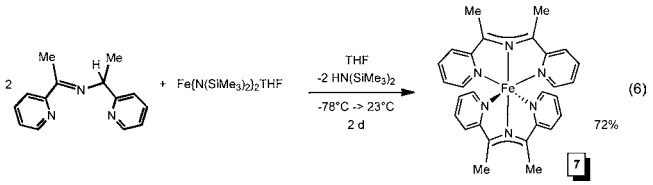

(6)

Surprisingly, the addition of 1 equiv of (^{b}Me$_2$smif)H to Fe{N(SiMe$_3$)$_2$}$_2$THF did not provide (^{b}Me$_2$smif)FeN(SiMe$_3$)$_2$ despite NMR tube scale reactions that showed a promising dark green color, and one dominant paramagnetic species by ^{1}H NMR spectroscopy. To check whether ^{b}Me$_2$smif was a viable ligand, 2 equiv of the imine precursor was added to Fe{N(SiMe$_3$)$_2$}$_2$THF, and diamagnetic, mossy green (^{b}Me$_2$-smif)$_2$Fe (**7**) was isolated in 72% yield (eq 6).

Potential problems affiliated with the methylated backbone were identified when a switch to (^{b}Me$_2$^{o}Me$_2$smif)H was conducted. The standard protocol failed to generate the desired monomeric product (^{b}Me$_2$^{o}Me$_2$smif)FeN(SiMe$_3$)$_2$ (**8**), although a dark green solution typical for smif-chelated iron complexes was generated.[5] As eq 7 illustrates, a red-orange

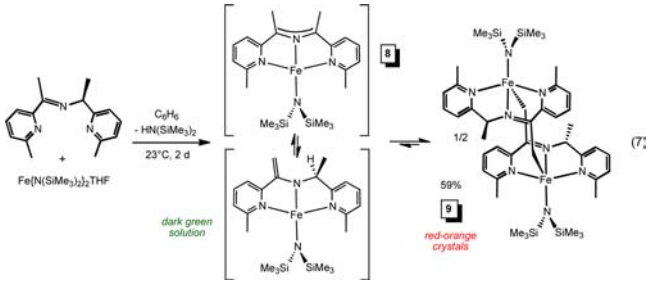

(7)

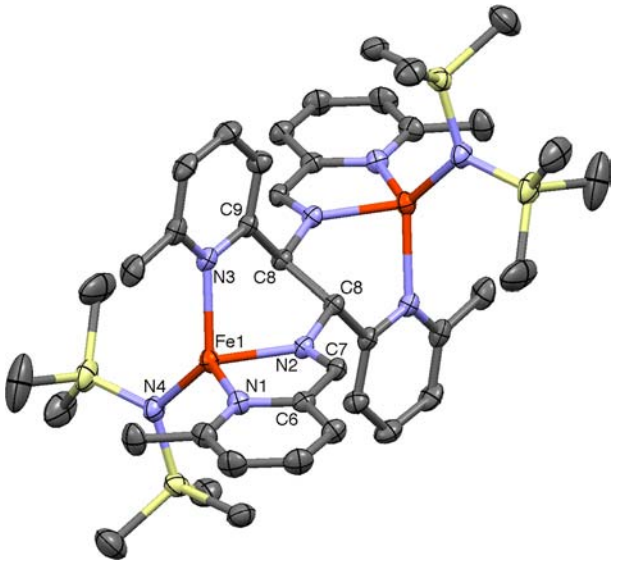

Figure 5. Molecular view of [{(Me$_3$Si)$_2$N}Fe]$_2$(μ:κ^3-*N*,py,py′,κ^3-*N*′,py′,py-^{o}Me$_2$smif-^{o}Me$_2$smif) (**6**). Selected interatomic distances (Å) and angles (deg): Fe−Fe, 5.941(2); Fe−N1, 2.0965(15); Fe−N2, 2.0069(15); Fe−N3, 2.1464(15); Fe−N4, 1.9489(15); N1−C6, 1.381(2); C6−C7, 1.405(3); N2−C7, 1.328(2); N2−C8, 1.448(2); C8−C8, 1.561(2); N1−Fe−N2, 79.19(6); N1−Fe−N3, 108.95(6); N1−Fe−N4, 118.19(7); N2−Fe−N3, 83.70(6); N2−Fe−N4, 129.78(6); N3−Fe−N4, 125.16(6); C7−N2−C8, 118.73(15); N2−C8−C8, 107.79(17); C8−C8−C9, 109.72(17).

dx.doi.org/10.1021/ic302783y | Inorg. Chem. 2013, 52, 3295−3312

dimer crystallized from benzene solution over a period of 2 days, but this species did not have any new C−C bonds. Figure 1 illustrated how the azaallyl anion can serve as a nucleophilic or electrophilic (or Lewis base/Lewis acid) functionality, and the dimer resulting from utilization of (^{b}Me$_2$^{o}Me$_2$smif) arises from a proton transfer from a backbone methyl group to a basic azaallyl carbon. The result of this process is an exomethylene group flanking an amide whose other adjacent site is a CHMe segment. Reversible dimerization of **8** occurs as two Fe−C bonds convert the two amides to imines, thereby retaining the Fe(II) oxidation states of the two centers. Dimer [{(Me$_3$Si)$_2$N}Fe]$_2$(μ-κ^4,κ^4-*N*,py$_2$,C-(^{b}Me,^{b}CH$_2$,^{o}Me$_2$(smif)H))$_2$ (**9**) was identified by single-crystal X-ray crystallography, while ^{1}H NMR spectra of redissolved **9** were consistent with the monomer, **8**.

The ferrous centers of **9** are potentially close enough (4.7420(5) Å) for a minimal interaction, and SQUID magnetometry data (Figure 6) revealed a declining μ_{eff} from

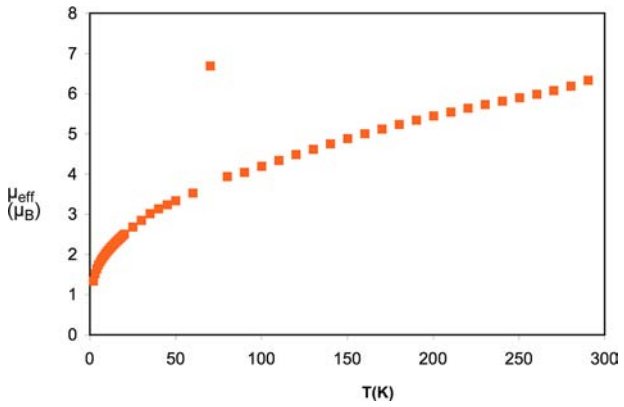

Figure 6. Plot of μ_{eff} vs T (K) for dimer [{(Me$_3$Si)$_2$N}Fe]$_2$(μ-κ^4,κ^4-*N*,py$_2$,C-(^{b}Me,^{b}CH$_2$,^{o}Me$_2$(smif)H))$_2$ (**9**).

6.3 μ_B at 293 K to ~3.0 μ_B at 50 K where the effects of ZFS appear. A μ_{eff} value of 6.93 μ_B is expected for two noninteracting Fe(II) S = 2 centers, and the decline observed is consistent with weak antiferromagnetic coupling (AF). It is also likely that the measurements reflect a high density of magnetic states present in the system.[34]

*2.1.7. Structure of [{(Me$_3$Si)$_2$N}Fe]$_2$(μ-κ^4,κ^4-N,py$_2$,C-(^{b}Me,^{b}CH$_2$,^{o}Me$_2$(smif)H))$_2$ (**9**).* Figure 7 depicts a molecular view of [{(Me$_3$Si)$_2$N}Fe]$_2$(μ-κ^4,κ^4-*N*,py$_2$,C-(^{b}Me,^{b}CH$_2$,^{o}Me$_2$(smif)H))$_2$ (**9**), where its inversion center can be readily seen. Metric parameters are given in the caption, and some structure solution details can be found in Table 1. The local structure about each iron is a distorted square pyramid, with the N(SiMe$_3$)$_2$ group bent 116.64(7)° away from the pseudoapical, elongated iron−carbon bond (2.336(2) Å), which is slightly bent away from the imine (106.59(7)°) and pyridine (91.07(7)°, 93.39(7)°) nitrogens. On the imine side of the plane, the Fe−N$_{py}$ distance is shorter (2.3192(17) Å) than that on the opposing arm of the ligand (2.3538(17) Å), and the chelate bite of 149.14(6)° is correspondingly small as compared to (smif)$_2$M derivatives, with ∠N1−Fe−N2 = 75.18(6)° and ∠N2−Fe−N3 = 74.29(6)°. The N$_{py}$−Fe−N$_{am}$ angles are 102.19(6)° and 102.96(6)°, and reflect the cant of the N(SiMe$_3$)$_2$ group out of the pseudo-N$_4$Fe plane.

Distances found for the former smif backbone are in between that of the *imine-alkyl* and *amide-exo-CH$_2$* forms depicted in Figure 7. The CN distance is 1.331(2) Å, which is long for a

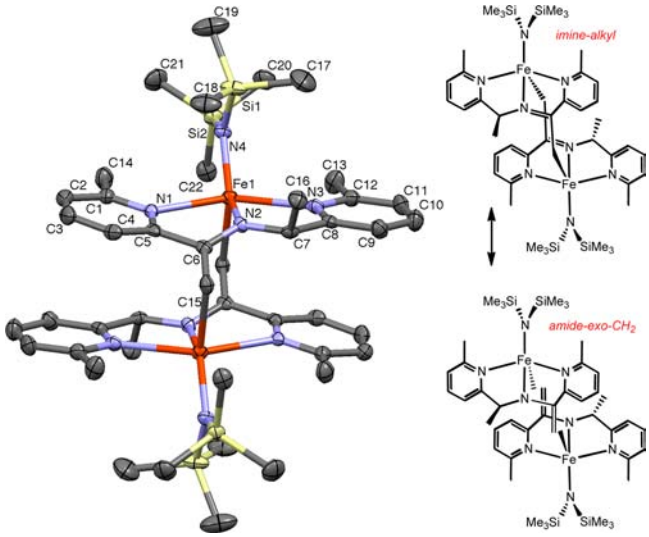

Figure 7. Molecular view of [{(Me$_3$Si)$_2$N}Fe]$_2$(μ-κ^4,κ^4-*N*,py$_2$,C-(^{b}Me,^{b}CH$_2$,^{o}Me$_2$(smif)H))$_2$ (**9**) and plausible valence bond structures. Selected interatomic distances (Å) and angles (deg): Fe−Fe, 4.7420(5); Fe−N1, 2.3192(17); Fe−N2, 2.0511(15); Fe−N3, 2.3538(17); Fe−N4, 1.9914(16); Fe−C15′, 2.336(2); Fe−C6′, 2.889(2); N2−C6, 1.331(2); N2−C7, 1.465(3); C6−C15, 1.375(3); N1−Fe−N2, 75.18(6); N1−Fe−N3, 149.14(6); N1−Fe−N4, 102.19(6); N2−Fe−N3, 74.29(6); N2−Fe−N4, 136.76(7); N3−Fe−N4, 102.96(6); N1−Fe−C15′, 91.07(7); N2−Fe−C15′, 106.59(7); N3−Fe−C15′, 93.39(7); N4−Fe−C15′, 116.64(7).

C═N double bond (cf 1.28 Å), and the d(CCH$_2$) is 1.375(5) Å, which is slightly long for a C═C bond (cf 1.33 Å), and quite short for a CC single bond. Consideration of the Fe−N2 interaction as an amide would suggest that the irons are ligated by an olefin, but in this case, the β-carbon is 2.889(2) Å away. Since this olefin is really an ene-amide, a disproportionately greater interaction with the α-carbon might be expected, and differentiation between the two valence bond depictions is moot.

2.2. Reactivity of the smif Backbone with Unsaturated Substrates. *2.2.1. 3 + 2 Cyclizations.* Figure 1 suggests that the CNC^{nb} orbital of a smif ligand can be considered as a reagent in C−C bond-forming reactions,[35−38] hence a variety of substrates potentially subject to nucleophilic, electrophilic, and radical reactivity were probed with limited success. Two distinct types of substrates provided isolable products, one of which was alkynes.[35] Treatment of a benzene solution of (smif)Fe{N(SiMe$_3$)$_2$} (**1**) with 2 equiv of ditolyl-acetylene afforded a dark green solution containing a mixture of compounds that included hexatolylbenzene (~15%). Crystallization from diethyl ether provided a red 3 + 2 cycloaddition product, [{2,5-di(pyrindin-2-yl)-3,4-di-(*p*-tolyl-2,5-dihydropyrrol-1-ide)}FeN(SiMe$_3$)$_2$]$_2$ (**11**, 19%) that was identified by X-ray crystallography. The yield of red crystals from a green solution was suggestive of another monomer/dimer situation, but direct evidence of a solution monomer, that is, {2,5-di(pyrindin-2-yl)-3,4-di-(*p*-tolyl-2,5-dihydropyrrol-1-ide)}FeN(SiMe$_3$)$_2$ (**10**), proved difficult to obtain due to the presence of other species. Utilization of 4 equiv of tolCCtol on an NMR tube scale in C$_6$D$_6$ permitted some of the reaction complexity to be unraveled, as one diamagnetic product was of high symmetry, and was tentatively identified as {2,5-di(2-pyridyl)-3,4-di-(*p*-tolyl)-pyrrolide}$_2$Fe (**12**).[39] Accompanying this product were *cis*- and *trans*-ditolyl-ethylene, which, along with **12**, suggested

dx.doi.org/10.1021/ic302783y | Inorg. Chem. 2013, 52, 3295−3312

that the CNC backbone of the dihydropyrrole unit of **10** could serve to transfer dihydrogen to ditolyl-acetylene. A subsequent disproportionation provided a plausible route to **12**.

SQUID magnetometry was conducted on **11**, but its interpretation is nontrivial. At 300 K, the μ_{eff} was ~5.3 μ_B, which is already substantially below that expected for two noninteracting Fe(II) centers (6.93), and well below the 8.94 μ_B that would represent an S_T = 4 system. A steady decline in μ_{eff} was observed until 25 K, where a modest flat discontinuity surfaced ~2.4 μ_B prior to the effects of ZFS. In systems, such as this, the low-symmetry and high-spin nature of the Fe(II) centers can lead to a high density of magnetic states, and a discussion of the case and alternative views are given in the Supporting Information. Nonetheless, the SQUID data are consistent with interacting Fe(II) centers, as the *d*(Fe−Fe) of 3.054 Å would suggest.

2.2.2. Structure of [{2,5-Di(pyrindin-2-yl)-3,4-di-(p-tolyl-2,5-dihydropyrrol-1-ide)}FeN(SiMe$_3$)$_2$]$_2$ (11). Data affiliated with the structure determination of **11** is given in Table 1, while selected metric parameters are presented in the caption of Figure 8, which provides molecular views of the molecule. The amide of the dihydropyrrol unit asymmetrically bridges the two irons with *d*(Fe−N) averaging 2.107(14) and 2.162(2) Å. The diamond core of the dimer is nearly square, with the Fe−N−Fe and N−Fe−N angles averaging 91.3(3)° and 88.3(4)°, respectively. The pyridines, while occupying differing sites, have iron−nitrogen bonds that average 2.158(16) Å, and the $(Me_3Si)_2N$ groups have the shortest bonds to iron, with *d*(Fe−N)$_{ave}$ = 2.060(6) Å, which is typical. Each iron is roughly embedded in a distorted square-pyramidal environment, with the $(Me_3Si)_2N$, the two pyridines, and the μ-dihydropyrrol occupying the basal sites, while the other, slightly shorter, μ-dihydropyrrolyl linkage is axial. The irregularity of the structure is noted through N_{ax}−Fe−N_{bas} angles ranging from the μ-dihydropyrrolyls at 88.57(5)° and 87.97(5)° to the $(Me_3Si)_2N$ groups at 114.51(6)° and 114.76(6)°.

2.2.3. Nucleophilic Attack of Isocyanates. While electrophilic substrates, such as aldehydes, ketones, CO_2, etc.,[35−38] failed to elicit reactivity from selected smif-containing complexes, principally $(smif)_2Fe$ (**13**), both ^{t}BuNCO and $(2,6\text{-}^i Pr_2C_6H_3)$NCO reacted with the CNC backbone of the smif ligands on **13**. As eq 8 indicates, dark red diamagnetic

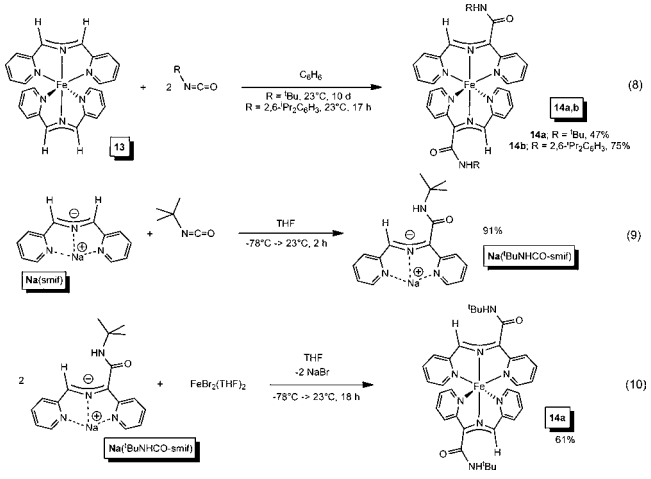

products $(RNHCO\text{-}smif)_2Fe$ (**14a**, R = ^{t}Bu, 47%; **14b**, 2,6-^{i}PrC$_6$H$_3$, 75%) resulted from nucleophilic attack from a carbon position on the smif backbone, followed by a proton transfer to the nitrogen of the isocyanate fragment.

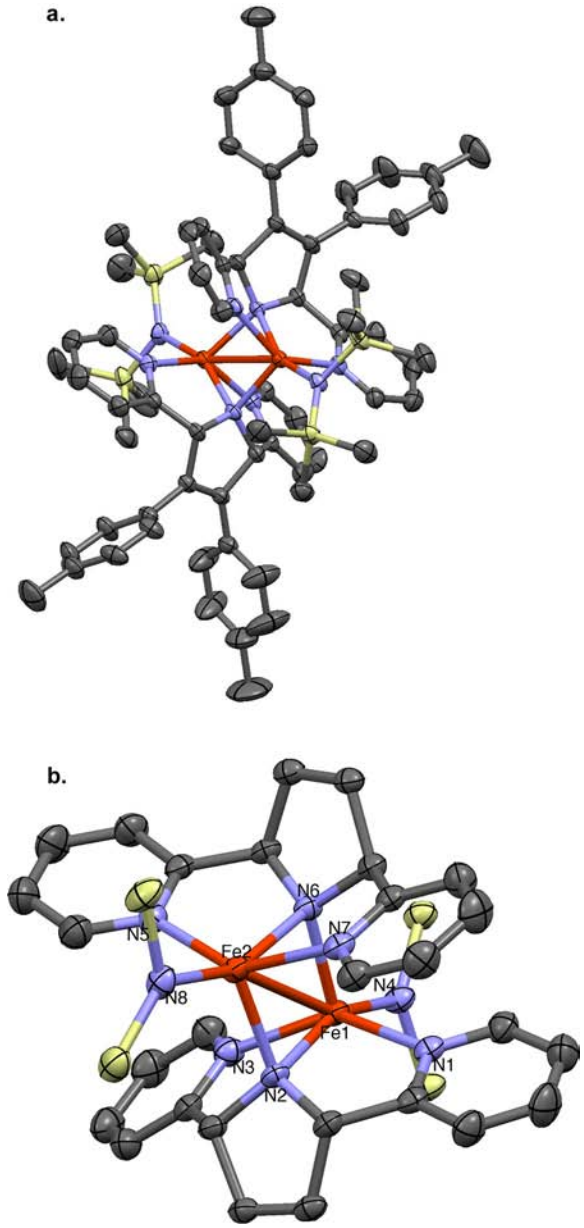

Figure 8. Molecular and truncated views of [{2,5-di(pyrindin-2-yl)-3,4-di-(*p*-tolyl-2,5-dihydropyrrol-1-ide)}FeN(SiMe$_3$)$_2$]$_2$ (**11**). Selected interatomic distances (Å) and angles (deg): Fe1−Fe2, 3.054; Fe1−N1, 2.1411(15); Fe1−N2, 2.1610(15); Fe1−N3, 2.1632(15); Fe1−N4, 2.0560(15); Fe1−N6, 2.0966(14); Fe2−N2, 2.1167(14); Fe2−N5, 2.1775(15); Fe2−N6, 2.1638(15); Fe2−N7, 2.1500(15); Fe2−N8, 2.0646(15); Fe1−N2−Fe2, 91.10(5); Fe1−N6−Fe2, 91.57(5); N1−Fe1−N2, 78.27(6); N1−Fe1−N3, 143.98(6); N1−Fe1−N4, 96.20(6); N2−Fe1−Fe3, 76.49(6); N2−Fe1−N4, 156.89(6); N3−Fe1−N4, 97.02(6); N6−Fe1−N1, 98.10(5); N6−Fe1−N2, 88.57(5); N6−Fe1−N3, 106.48(6); N6−Fe1−N4, 114.51(6); N5−Fe2−N6, 76.43(6); N5−Fe2−N7, 144.10(6); N5−Fe2−N8, 97.02(6); N6−Fe2−N7, 77.88(5); N6−Fe2−N8, 157.21(6); N7−Fe2−N8, 97.05(6); N2−Fe2−N5, 107.18(6); N2−Fe2−N6, 87.97(5); N2−Fe2−N7, 96.48(5); N2−Fe2−N8, 114.76(6).

Since the azaallyl anion functionality should behave as a nucleophile,[35] Na(smif) was treated with ^{t}BuNCO, resulting in a deep red solution from which Na(^{t}BuNHCO-smif) was obtained as metallic green microcrystals in 91% yield (eq 9). As

dx.doi.org/10.1021/ic302783y | Inorg. Chem. 2013, 52, 3295−3312

an alternative route to (^{t}BuNHCO-smif)$_2$Fe (**14a**), the addition of 2 equiv of Na(^{t}BuNHCO-smif) to FeBr$_2$(THF)$_2$ in THF resulted in a dark red-orange solution, from which the complex was isolated in 61% yield as dark red crystals (eq 10). Attachment of the amide groups to the smif backbone may become important if these optically dense materials need to be incorporated into a polymer for light-harvesting applications. Condensation polymerization of **14a**,**14b** with a diammine or the elaboration of (smif)$_2$M with a diisocyanate constitute two plausible paths based on eqs 8−10.

In regard to UV−vis spectroscopy, inclusion of backbone amides causes a blue shift in the "red" intraligand (IL) bands from that of (smif)$_2$Fe (**13**-Fe, $\lambda_{max} \sim 603$ nm), as the λ_{max} for **14a** is at 525 nm ($\varepsilon \sim 21\,000$ M^{-1} cm^{-1}), and that of **14b** is at 530 nm ($\varepsilon \sim 22\,000$ M^{-1} cm^{-1}). This shift changes the color of the compounds from the dark green of **13** to the dark red hues of **14a**,**14b**, and unmasks bands at 638 nm ($\varepsilon \sim 7000$ M^{-1} cm^{-1}) and 644 nm ($\varepsilon \sim 6000$ M^{-1} cm^{-1}) for **14a** and **14b**, respectively, that are tentatively assigned as lower-symmetry components of CNC^{nb} → smif-π^* transitions[5,6] generated from amide substitution. The "blue" IL bands of **14a** at 431 nm ($\varepsilon \sim 42\,000$ M^{-1} cm^{-1}) and **14b** at 427 nm ($\varepsilon \sim 46\,000$ M^{-1} cm^{-1}) change only slightly from the $\lambda_{max} \sim 437$ nm ($\varepsilon \sim 42\,000$ M^{-1} cm^{-1}) for **13**.

*2.2.4. Structure of (2,6-iPrC$_6$H$_3$-NHCO-smif)$_2$Fe (**14b**).* A listing of particular structure refinement and collection data can be found in Table 1, while selected metric parameters are given in the caption to Figure 9, which illustrates the C_2 symmetry of (2,6-^{i}PrC$_6$H$_3$-NHCO-smif)$_2$Fe (**14b**). Core distances attributed to **14b** are very similar to (smif)$_2$Fe (**13**),[5] with Fe−N$_{aza}$ bond lengths averaging 1.908(11) Å, and d(Fe−N$_{py}$) averaging 1.955(14) Å. The FeN$_6$ core is nearly D_{2d}, with ∠N$_{aza}$−Fe−N$_{aza}$ = 176.49(17)°, N$_{aza}$−Fe−N$_{py}$ angles averaging 83.1(4)°, N$_{py}$−Fe−N$_{py}$ angles of 165.92(16)° (ave), N$_{py}$−Fe−N′$_{py}$ angles of 90.8(18)° (ave), and a very modest spread (94.00(16)−99.96(16)°) in N$_{aza}$−Fe−N′$_{py}$ angles. The amide electron-withdrawing group renders the CNC linkage asymmetric. The d(CN) away from the amide is short (1.329(11) Å ave) compared to the CN adjacent to the amide (1.366(8) Å ave), and the CC bond connecting the amide to the smif backbones is slightly shorter (1.446(7) Å) than expected (1.47 Å), consistent with some delocalization of charge into the amide. The remaining metric parameters in the molecule are ordinary.

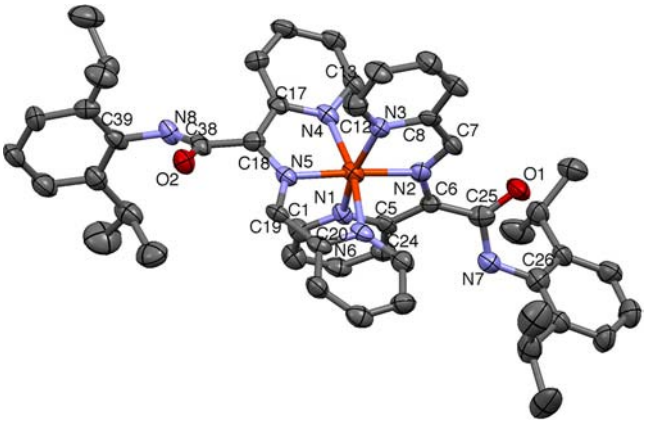

Figure 9. Molecular and truncated views of (2,6-^{i}PrC$_6$H$_3$-NHCO-smif)$_2$Fe (**14b**). Selected interatomic distances (Å) and angles (deg): Fe−N1, 1.948(4); Fe−N2, 1.900(4); Fe−N3, 1.956(4); Fe−N4, 1.941(4); Fe−N5, 1.916(4); Fe−N6, 1.974(4); N2−C6, 1.371(6); N2−C7, 1.337(6); N5−C18, 1.360(6); N5−C19, 1.321(6); C6−C25, 1.446(7); C18−C38, 1.446(7); N1−Fe−N2, 83.07(16); N1−Fe−N3, 165.81(16); N1−Fe−N4, 90.01(15); N1−Fe−N5, 97.46(16); N1−Fe−N6, 91.10(15); N2−Fe−N3, 83.17(16); N2−Fe−N4, 99.96(15); N2−Fe−N5, 176.49(17); N2−Fe−N6, 94.00(16); N3−Fe−N4, 89.00(15); N3−Fe−N5, 96.48(16); N3−Fe−N6, 93.27(15); N4−Fe−N5, 83.52(16); N4−Fe−N6, 166.03(17); N5−Fe−N6, 82.53(16); Fe−N2−C6, 115.4(3); Fe−N2−C7, 115.8(3); Fe−N5−C18, 115.8(3); Fe−N5−C19, 115.5(3).

2.3. Collateral Discovery − Alkyne Cyclotrimerization by {(Me$_3$Si)$_2$N}$_2$Fe(THF). While investigating the 3 + 2 cyclization[35] of ditolyl-acetylene to (smif)Fe{N(SiMe$_3$)$_2$} (**1**) illustrated in Scheme 1, the presence of hexa-tolyl-benzene was noted, an obvious consequence of alkyne cyclotrimerization.[40−48] As a consequence, a variety of smif- and dpma-containing compounds were tested for catalytic activity with 2-butyne as the substrate. Of these compounds tested, **1** proved to be the best (Table 2), but evidence of degradation during cyclotrimerization suggested that other species might warrant consideration. For example, roughly 20−30% of **1** remained after 50 equiv of 2-butyne was cyclotrimerized, according to several trials, and evidence of HNSi(Me$_3$)$_2$ and (smif)$_2$Fe (**13**) was obtained by ^{1}H NMR spectroscopy. Accordingly, {(Me$_3$Si)$_2$N}$_2$Fe(THF) was considered as a potential catalyst[48] since the reactivity shown in Scheme 1 revealed that the CNC backbone of smif would react with the alkyne, potentially triggering disproportionation events. Table 1 shows that {(Me$_3$Si)$_2$N}$_2$Fe(THF) is a superior catalyst for the conversion of 2-butyne to hexamethylbenzene, with a TOF of ∼10 h^{-1} at 2 mol % catalyst loadings at 90 °C, with little or no apparent degradation. The results are quite comparable to other cyclotrimerization catalysts.[45,48] Whereas the crude data suggests that the cyclotrimerization is first-order in the catalyst, the order in the substrate is unclear at this juncture.

2.4. Collateral Discovery − Dihydrogen Transfer from dpma. *2.4.1. Calculations on H$_2$ Loss from dpma.* The tentative identification of {2,5-di(2-pyridyl)-3,4-di-(*p*-tolyl)-pyrrolide}$_2$Fe (**12**), accompanied by alkyne hydrogenation products (Scheme 1) suggested that saturating a smif backbone, that is, conversion to an amide, could lead to dihydrogen transfer. The thermodynamics of such an event was investigated via DFT calculations, as indicated in Scheme 2, where the dehydrogenation of D_{2d} (dpma)$_2$Fe (**15**) to (smif)$_2$Fe (**13**) and 2 H$_2$ was examined. The dehydrogenation is roughly thermoneutral, as loss of the first equivalent of dihydrogen is slightly endothermic (1.1 kcal/mol), whereas the loss of the second equivalent is slightly exothermic (−2.9 kcal/mol). The favorable free energy of reaction ($\Delta G^\circ = -12.5$ kcal/mol) is due mostly to the increase in entropy ($\Delta S^\circ = 36$ eu) as the 2 equiv of dihydrogen are released. Since **15** is a high-spin complex, the stepwise conversion also reflects a change in spin state en route to **13**. According to the calculations, (dpma)-(smif)Fe (**16**) is also $S = 2$; hence the spin state change to $S = 0$ occurs in the second dehydrogenation. The second entropy change is likely attenuated due to the spin state change, and the overall greater rigidity of the low-spin bis-smif derivative.

*2.4.2. Synthesis and Characterization of (dpma)$_2$Fe (**15**).* Treatment of {(Me$_3$Si)$_2$N}$_2$Fe(THF) with 2 equiv of (dpma)H in diethyl ether afforded dark blue (dpma)$_2$Fe (**15**) in 75% yield according to eq 11. An Evans' method magnetic measurement on **15** ($\mu_{eff} = 5.0\ \mu_B$) and SQUID magnetometry measurements(μ_{eff} (290 K) = 5.2 μ_B) are consistent with a relatively symmetric $S = 2$ center, since the effects of ZFS are

dx.doi.org/10.1021/ic302783y | Inorg. Chem. 2013, 52, 3295−3312

Scheme 1

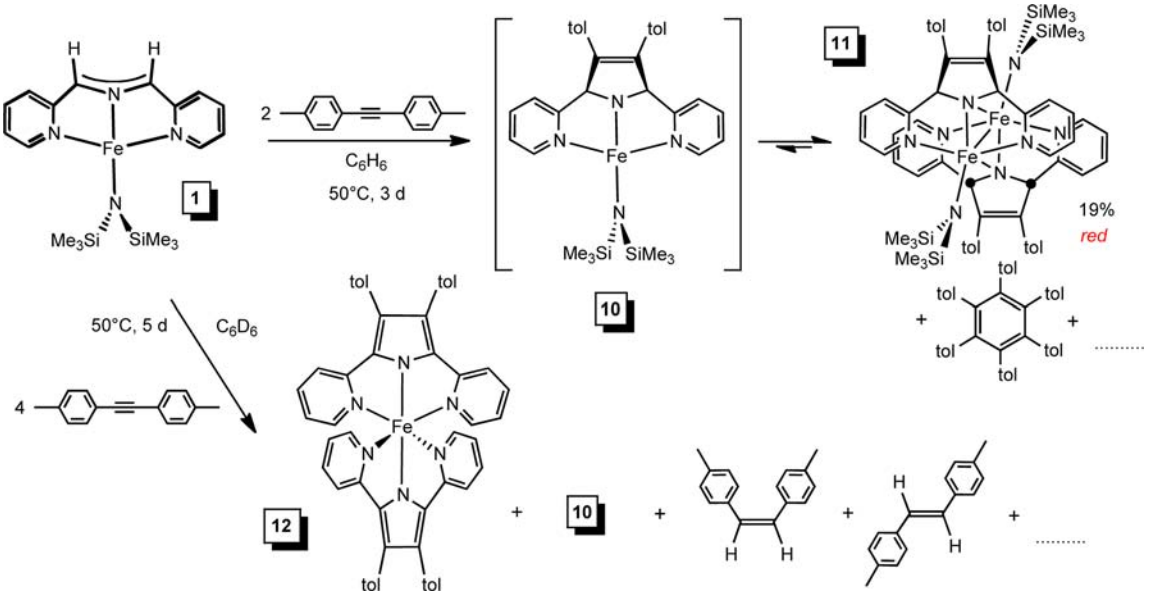

Table 2. Catalytic Cyclotrimerization Results for the Conversion of 2-Butyne to Hexamethylbenzene with (smif)Fe{N(SiMe$_3$)$_2$} (1) or {(Me$_3$Si)$_2$N}$_2$Fe(THF)

trial	cat.	cat. mol. %	[cat.] × 10^3 M	T (°C)	TON	TOF (h^{-1})[a]
1	{(Me$_3$Si)$_2$N}$_2$Fe(THF)	1.6	4.5	75	60	4.4
2	{(Me$_3$Si)$_2$N}$_2$Fe(THF)	2	4.5	90	50	3.7
3	{(Me$_3$Si)$_2$N}$_2$Fe(THF)	2	9.0	90	50	10
4	{(Me$_3$Si)$_2$N}$_2$Fe(THF)	2	13.5	90	52	10.4
5[b]	(smif)Fe{N(SiMe$_3$)$_2$} (**1**)	2	4.8	75	14	0.31
6[c]	(smif)Fe{N(SiMe$_3$)$_2$} (**1**)	2	4.8	90	12	1.1
7[d]	(smif)Fe{N(SiMe$_3$)$_2$} (**1**)	2	9.7	90	50	7.4
8[e]	(smif)Fe{N(SiMe$_3$)$_2$} (**1**)	1.6	14.5	90	60	8.9
9	LiN(TMS)$_2$	2	36	90	0	0
10	FeBr$_2$(THF)$_2$	2	17	90	0	0

[a]Assessed at short reaction times such that [2-butyne] complies with pseudo-first-order conditions. [b]20% **1** remained at conclusion. [c]23% **1** remained at conclusion. [d]29% **1** remained at conclusion. [e]24% **1** remained at conclusion.

Scheme 2

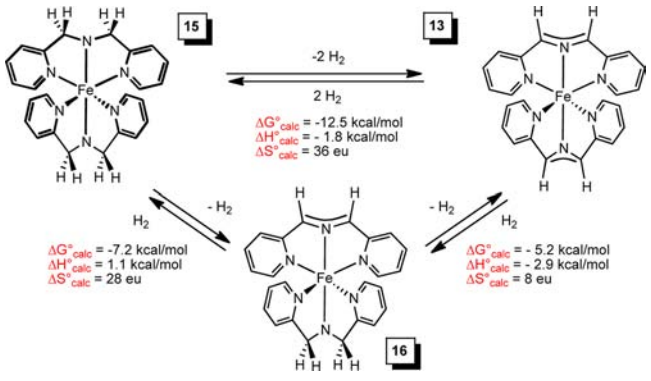

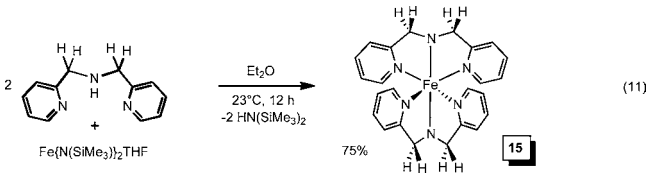

(11)

seen below 50 K (Figure 10). The Mössbauer spectrum of **15** supports this conclusion, as the isomer shift of 0.94 mm/s is typical for high-spin Fe(II), and the quadrupole splitting value is a modest 0.86 mm/s, indicative of a relatively symmetric electronic environment.[23,24] Crystals of (dpma)$_2$Fe (**15**) were orthorhombic, with two independent, statistically equivalent molecules in the asymmetric unit. A view of one molecule is given in Figure 10, while selected details regarding data collection and refinement are given in Table 1. The aza nitrogens average 2.001(13) Å from the iron, and are 175.9(16)° (ave) apart, whereas the pyridine nitrogens average 2.201(13) Å, and are 150.9(16)° (ave) apart. The N_{aza}–Fe–N_{py} intrachelate angles average 75.5(4)°, while significant variation is observed for the N_{aza}–Fe–N_{py}' and N_{py}–Fe–N_{py}' angles between opposing dpma ligands, which range from 99.8(2) to 109.5(2)° and 86.90(7) to 101.00(7)°, respectively. The Fe–N_{aza} and Fe–N_{py} distances are 0.10 and 0.24 Å greater than the corresponding (smif)$_2$Fe (**13**) derivative, an indication of the significantly weaker field affected by dpma versus smif.

Subsequent to the initial structural reports of (smif)$_2$Fe (**13**) and (dpma)$_2$Fe (**15**),[4] Westerhausen et al. also published the results of X-ray crystallographic studies on both complexes.[26]

dx.doi.org/10.1021/ic302783y | Inorg. Chem. 2013, 52, 3295–3312

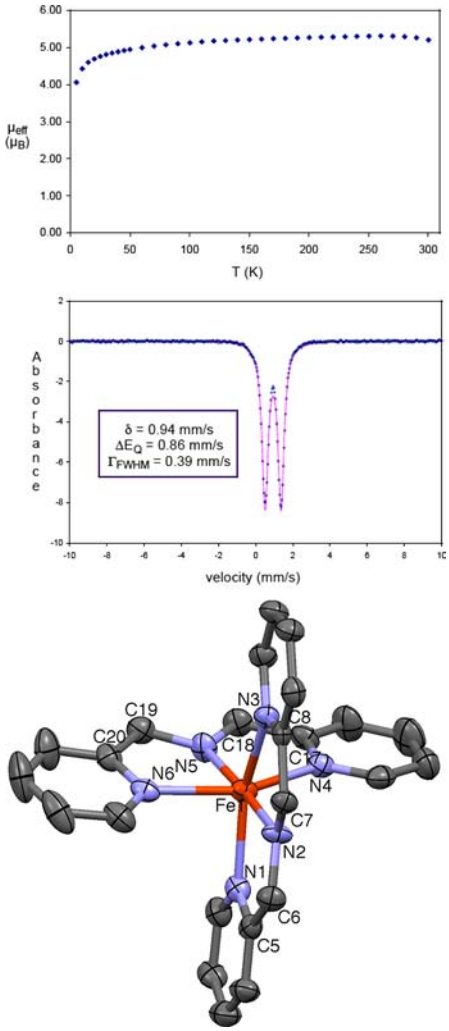

Figure 10. Plot of μ_{eff} vs T (K) for $(dpma)_2Fe$ (**15**) showing its $S = 2$ GS. Mössbauer spectrum that is consistent with an $S = 2$ GS, and a view of one molecule of the asymmetric unit. Selected interatomic distances (Å) and angles (deg): Fe1−N1, 2.197(2); Fe1−N2, 2.0184(18); Fe1−N3, 2.194(2); Fe1−N4, 2.195(2); Fe1−N5, 1.9921(18); Fe1−N6, 2.197(2); N2−C6, 1.421(3); N2−C7, 1.417(3); N5−C18, 1.417(3); N5−C19, 1.418(3); N1−Fe1−N2, 75.44(8); N1−Fe1−N3, 150.82(7); N1−Fe1−N4, 98.88(8); N1−Fe1−N5, 105.07(8); N1−Fe1−N6, 89.65(8); N2−Fe1−N3, 75.40(8); N2−Fe1−N4, 109.47(8); N2−Fe1−N5, 174.72(8); N2−Fe1−N6, 99.75(8); N3−Fe1−N4, 91.76(8); N3−Fe1−N5, 103.87(8); N3−Fe1−N6, 94.20(7); N4−Fe1−N5, 75.73(7); N4−Fe1−N6, 150.75(7); N5−Fe1−N6, 75.04(8). Related distances and angles of the second molecule are statistically indistinguishable.

There are no substantial conflicts when the metric parameters of the two independent studies are compared.

2.4.3. dpma Backbone Dihydrogen Transfers. The potential to dehydrogenate the $-CH_2$-N-CH_2- backbone of the dpma ligands in $(dpma)_2Fe$ (**15**) was tested via a series of NMR tube scale experiments where the products could be readily assayed. As shown in Scheme 3, numerous transfers were observed, but the $(smif)_2Fe$ (**13**) product was unable to be recycled back to **15** via H_2 or other dihydrogen sources, thereby preventing catalytic applications. In addition, (dpma)H (not shown) was often noted at the end of the reactions, perhaps indicative of protolytic degradation paths. Nonetheless, a variety of hydrogenations were noted, and mechanistic evaluations were attempted utilizing backbone-deuterated $(dpma\text{-}d_4)_2Fe$ (**15**-d_8; see the Supporting Information for a summary of the labeling studies).[49]

The addition of benzophenone to $(dpma)_2Fe$ (**15**) proved to be complicated, as at least two paramagnetic iron species formed in addition to $(smif)_2Fe$ (**13**). Treatment of (smif)-FeN$(SiMe_3)_2$ (**1**) with (dpma)H or exposure of (dpma)FeN-$(SiMe_3)_2$ (**3**) to (smif)H led to mixtures of (smif)(dpma)Fe (**16**) and $(smif)_2Fe$ (**13**) due to disproportionation processes, as shown in Scheme 4. The ^{1}H NMR spectrum of **16** was readily identified, yet it was not deemed to be a byproduct in the benzophenone reaction with **15** (**16** was present in a number of shorter duration studies with alkynes and imines; see the Supporting Information). It was logical that the products derived from protonation of iron amide bonds by Ph_2CHOH were present, since the free alcohol was not observed. Treatment of **3** with Ph_2CHOH permitted isolation of a plum-colored solid whose main ^{1}H NMR spectral resonances were consistent with $[(dpma)FeOCHPh_2]_n$ (**17**). Likewise, when Ph_2CHOH was added to **1**, a green solid was produced, and ^{1}H NMR spectral analysis indicated a rough 1:1 mixture of $[(smif)FeOCHPh_2]_n$ (**18**) and ubiquitous **13**. Aqueous quenches of **17** and **18** afforded Ph_2CHOH as a major product. Spectral comparisons showed that **17** was a product of Ph_2CO reduction by **15**, and a rough balancing of the observed products suggested that "$(Ph_2CHO)_2Fe$" may also be produced.[50]

When $(dpma)_2Fe$ (**15**) was exposed to excess 2-butyne or ditolyl-acetylene, hydrogenation to *cis*-alkenes were observed in addition to trimerization products hexamethylbenzene and hexatolylbenzene, and $(smif)_2Fe$ (**13**) was the identifiable iron-containing product. *Trans*-alkenes are also observed in the reaction mixtures, but subsequent studies showed that they could be generated in a post-hydrogenation isomerization event. The cyclotrimerization activity of **15** was determined to be worse than the catalysts tested in Table 2, but there is clearly a commonality of iron-amide functionalities.[46−48] ^{1}H NMR assays of product mixtures derived from the use of $(d_4\text{-}dpma)_2Fe$ (**15**-d_8) proved frustratingly difficult to decipher, and clean transfer of dideuterium to alkyne was not noted in any instance.

When $(dpma)_2Fe$ (**15**) was heated in the presence of *cis*-2-butene for an extended period (50 °C, ∼7 days), hydrogenation to *n*-butane was noted and some of the residual olefin was isomerized to *trans*-2-butene. Once again, the only iron-containing product identified by ^{1}H NMR spectroscopy was $(smif)_2Fe$ (**12**). Butadiene was also hydrogenated to a mix of 1-butene, and *cis*- and *trans*-2-butene, and **13** was again produced.

Unsaturated nitrogen-containing substrates proved to be some of the best in terms of conversion, as azobenzene and 3,6-mesityl-imino-1,4-cyclohexadiene[51] were smoothly converted by $(dpma)_2Fe$ (**15**) to 1,2-diphenylhydrazine and 1,4-dimesityl-imino-benzene as $(smif)_2Fe$ (**13**) formed. When $(d_4\text{-}dpma)_2Fe$ (**15**-d_8) was used, azobenzene was converted to PhND-NDPh, but the iron product, expected to be $(d_2\text{-}smif)_2Fe$ (**13**-d_4), had 2−6% H in its backbone. In addition, treatment of **15**-d_8 with 1,4-dimesitylamino-benzene afforded 1,4-$(MesND/H)_2$-C_6H_4[52] with 25−32% H in the amine positions. Silating the glassware lowered the amount to 16% H, but clearly, clean labeling studies were difficult to obtain, even with the better substrates. The imine PhCH═NBn and some simple variants were also chosen as substrates for **15**, but the reaction paths were less

dx.doi.org/10.1021/ic302783y | Inorg. Chem. 2013, 52, 3295−3312

Scheme 3

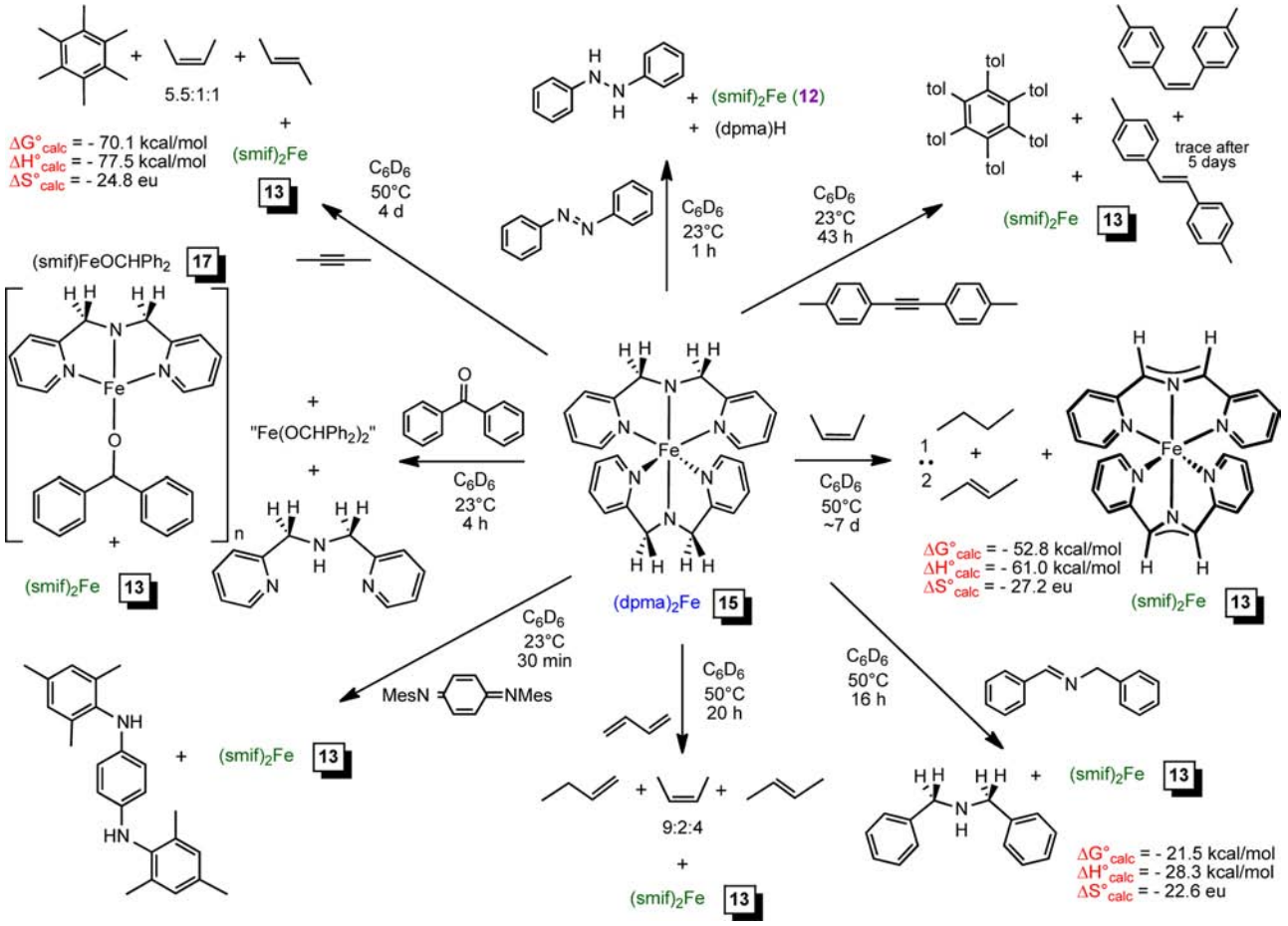

Scheme 4

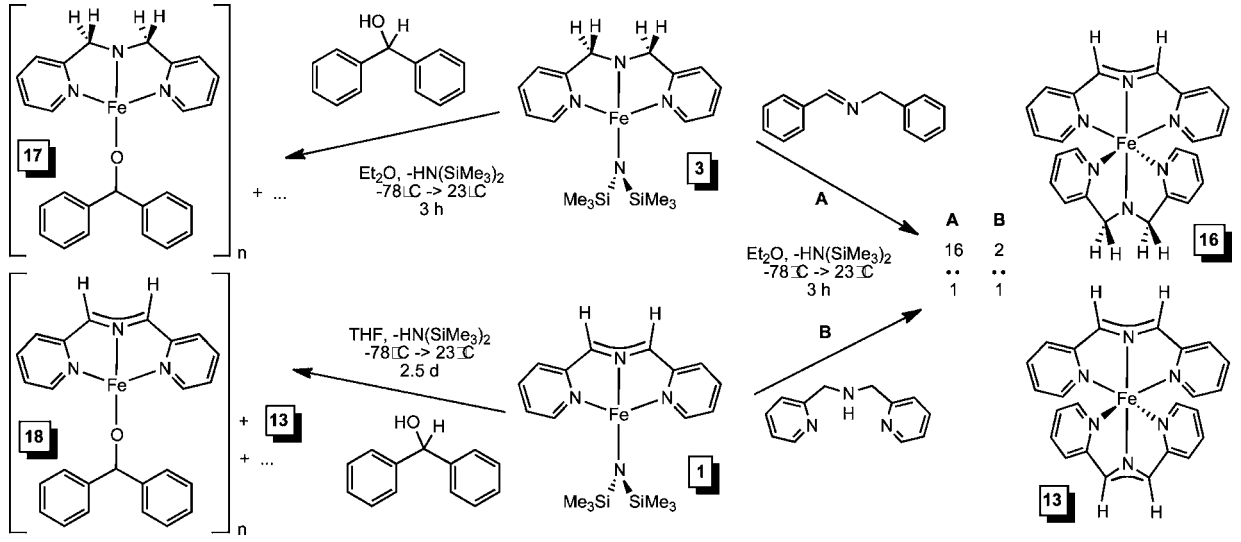

clean, as indicated by stoichiometry relative to a standard, reproducibility, and incomplete label transfer from **15**-d_8.

While a conclusive general path for the dehydrogenative events could not be established, there is a favorite among the three general processes—illustrated via alkyne reduction—depicted in Scheme 5. A radical would likely transfer H atoms in discrete steps to an alkyne, but the general lack of *trans*-olefin products in the early stages of reaction and the observation that *cis*-products do eventually isomerize discredit this mechanism, despite the stabilization of a metalaradical, such as **19**, due to its Fe(III) form. While a concerted dihydrogen transfer is attractive in terms of the initial *cis*-geometry, and its resemblance to the 2 + 3 cyclizations into the CNC smif backbone, scrambling of hydrogen into the smif ligands of product $(smif)_2Fe$ (**13**), albeit typically a modest amount, has been observed for certain substrates. The data, while difficult to

dx.doi.org/10.1021/ic302783y | Inorg. Chem. 2013, 52, 3295−3312

Scheme 5

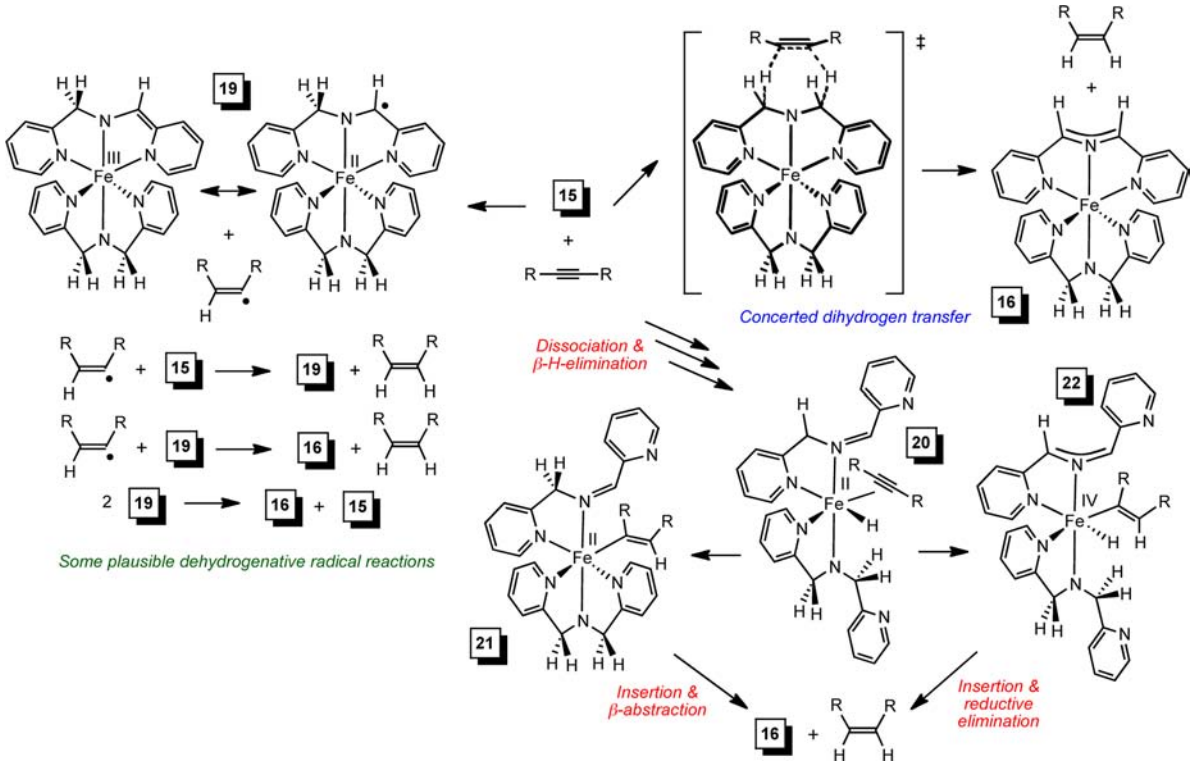

interpret due to the presence of paramagnetic species, overlapping resonances, etc., appears best accommodated by a standard β-H-elimination process that leads to **20**, followed by insertion to give **21** or **22**, and abstraction from the former Fe(II) species or reductive elimination from the putative Fe(IV) intermediate can lead to products.

Substrates 1,2-diphenylhydrazine and 1,4-dimesitylimino-benzene, the ones that react most cleanly, may be mechanistically different in that the rate of H_2/D_2 transfer is demonstrably faster (<1 h, 23 °C). In the former case, a substantial amount of (dpma)H is generated, and H (2−6%) is found in the backbone of the modest amount of **13**-d_4 produced. For the latter, (dpma)H is again produced, and the amount of H found in the 1,4-(MesND/H)$_2$-C_6H_4 product ranged from 16% to 32% depending on the run. The complexity of the process, as evident in virtually every trial, greatly hampered the formulation of concrete mechanistic conclusions (see the Supporting Information).

3. DISCUSSION

3.1. The Covalent Diradical Component of the CNC Backbone. The description of the CNC^{nb} orbital in Figure 1 as being composed of covalent diradical[53−58] and ionic components has been supported by reactivity at the coordinated smif ligand. A standard ambiguity persists when characterizing related singlet diradicals,[53−58] whose products in various reactions can also be ascribed to nucleophile/electrophile behavior. Similarly, dimerization of (smif)Fe{N(SiMe$_3$)$_2$} (**1**) to [{(Me$_3$Si)$_2$N}Fe]$_2$(μ-κ^3,κ^3-*N*,py$_2$-smif,smif) (**2**) can be ascribed to a radical coupling, or an attack of the smif anion on the electrophilic (imine) part of another, that is, the ionic view of the backbone. Nonetheless, this reversible C−C bond formation, perhaps hinted at in the elongated C−C bonds of 1.578(2) Å between the two CNC units, can justifiably be considered a radical coupling. A related aluminum complex has been generated as a byproduct in the thermolysis of (dpma)AlMe$_2$,[59] and it is plausible that (smif)AlMe$_2$ is a short-lived intermediate in this process.

Another example that can be interpreted as evidence of the covalent diradical character of the CNC^{nb} smif backbone is the 3 + 2 cycloaddition of ditolyl-acetylene to (smif)Fe{N(SiMe$_3$)$_2$} (**1**), which eventually affords the dimer [{2,5-di(pyrindin-2-yl)-3,4-di-(*p*-tolyl-2,5-dihydropyrrol-1-ide)}FeN(SiMe$_3$)$_2$]$_2$ (**11**). The relatively mild conditions under which the cyclization occurs and the lack of any dipolar nature to the alkyne support the plausibility of a reaction with diradical character. Furthermore, some of the dehydrogenations of (dpma)$_2$Fe (**15**), and the dehydrogenation of **11**, followed by disproportionation to yield the tentatively identified {2,5-di(2-pyridyl)-3,4-di-(*p*-tolyl)-pyrrolide}$_2$Fe (**12**, Scheme 1),[39] may be examples of H-atom abstraction that may point toward the diradical character of the smif-like ligands in the ultimate products.

Evidence of radical behavior pertaining to the CNC backbone is also evident in the coupling of putative (^{o}Me$_2$smif)FeN(SiMe$_3$)$_2$ (eq 4), in which the ^{o}Me$_2$smif ligand ends up spanning two iron centers as a single C−C bond is generated to form [{(Me$_3$Si)$_2$N}Fe]$_2$(μ:κ^3-*N*,py,py′,κ^3-*N*′,py′,py-^{o}Me$_2$smif-^{o}Me$_2$smif) (**6**). Here, it is likely that the *ortho*-methyl substituents on the smif labilize arms of the chelate, allowing it to bind two irons in the course of finding the configuration in which C−C bond formation via radical coupling can occur. Subsequently, the two Fe(I) cores generated via the reductive coupling process each reduce a pyridine-imine unit, and the ultimate oxidation state of each becomes Fe(II). Counter to the other C−C bond-forming processes, this is the only case in which metal redox events are critical.

dx.doi.org/10.1021/ic302783y | *Inorg. Chem.* 2013, 52, 3295−3312

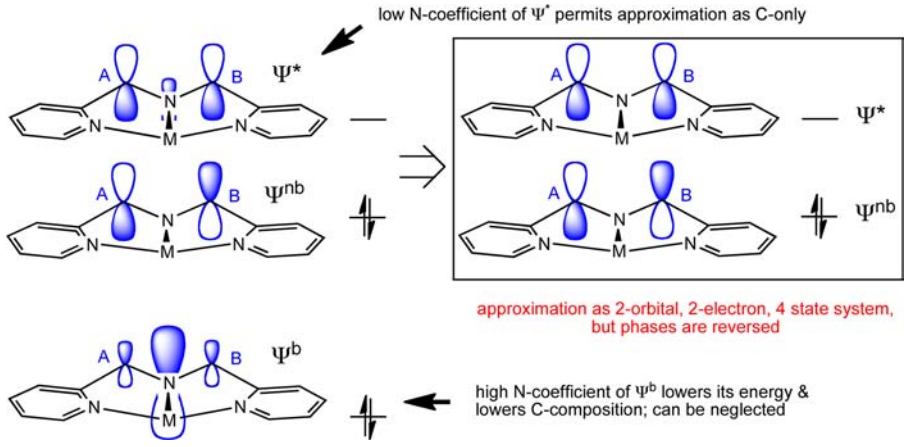

Figure 11.

3.2. The Ionic Component of the CNC Backbone. Attempts to prevent CNC backbone coupling reactions via methylation brought about interference from proton transfer, which can be interpreted as a consequence of the acid/base-like, or nucleophile/electrophile-like character of the functionality. The internal proton transfer involving (^{b}Me$_2$^{o}Me$_2$smif)-FeN(SiMe$_3$)$_2$ (**8**), which implicates the ionic nature of the CNC^{nb} backbone, causes a dimerization to [{(Me$_3$Si)$_2$N}Fe]$_2$-(μ-κ^4,κ^4-*N*,py$_2$,C-(^{b}Me,^{b}CH$_2$,^{o}Me$_2$(smif)H))$_2$ (**9**). A visualization of the process given in Figure 7 provides two resonance forms, an imine-alkyl and an amide-exomethylene, but the metric parameters favor the former. The dark green solution observed upon dissolving **9** is common for "(smif)Fe" moieties, and the accompanying ^{1}H NMR spectrum of the species in solution suggests that **8** is regenerated replete with a reversal of the proton transfer.

The most convincing evidence of the potential nucleophilic character of the CNC^{nb} orbital of the smif backbone is the clean attack of isocyanates ^{t}BuNCO and (2,6-^{i}Pr$_2$C$_6$H$_3$)NCO by (smif)$_2$Fe (**13**) to produce (RNHCO-smif)$_2$Fe (**14a**, R = ^{t}Bu; **14b**, 2,6-^{i}PrC$_6$H$_3$). Not only is the reaction a clear indication of the ionic character of the smif backbone, but it shows how smif-containing complexes can be readily incorporated into polymeric matrixes via cross-linking by diisocyanates.

3.3. Approximating the 2-Azaallyl Anion. In principle, treatments of allyl anions should manifest the same nonbonding orbital composition given in the simplified version of smif illustrated in Figure 1. In the calculations, an appreciable resonance stabilization is indicated,[60−64] and considerable ionic character is implied. The 2-azaallyl anion is distinguished by its central electronegative nitrogen, which changes the nature, and substantially changes the energies, of the standard 3 orbital, 4 electron, 15 state system. Figure 11 shows that the lowest allyl orbital is dominated by nitrogen character, whereas the antibonding allyl orbital is virtually all carbon in character. These features allow neglection of Ψ^b, and the approximation of Ψ^* permits the system to be assessed as a 2 orbital, 2 electron, 4 state system, albeit with the phases of the orbitals switched from a standard diradical.[65] The states arising from the $(\Psi^{nb})^2$ and $(\Psi^*)^2$ configurations interact to modulate the amount of ionic and covalent character in each, and the resulting ground state (GS), as described in Figure 1, has mostly ionic character, but retains some covalent diradical composition. Estimates based on a CASSCF(4,3)/6-31G(d) calculation of the ground state on the neutral model $H_2CN(+)HCH_2(-)$ suggest that ∼9% of its GS is a singlet diradical.

4. CONCLUSIONS

Chemical reactivity of smif-containing iron compounds supports the description of the CNC^{nb} backbone-localized orbital as having covalent diradical and/or ionic character. The reactions also show that, while pseudo-square-planar iron(II) complexes are becoming more common, without substantial steric features, the formation of dimers is to be expected. Collateral findings include the discovery that the common starting material {(Me$_3$Si)$_2$N}$_2$Fe(THF) is a significant alkyne cyclotrimerization catalyst, and that the saturated backbone of the related di-2-pyridyl-methyl-amide ligand can be readily dehydrogenated. The mechanism of the dehyrogenation of (dpma)$_2$Fe was not readily elucidated, and may depend on the nature of the substrate.

5. EXPERIMENTAL SECTION

5.1. General Considerations. All manipulations were performed using either glovebox or high-vacuum line techniques. All glassware was oven-dried. THF and ether were distilled under nitrogen from purple sodium benzophenone ketyl and vacuum transferred from the same prior to use. Hydrocarbon solvents were treated in the same manner with the addition of 1−2 mL/L tetraglyme. Benzene-d_6 and toluene-d_8 were dried over sodium, vacuum transferred, and stored over activated 4 Å molecular sieves. THF-d_8 was dried over sodium and vacuum transferred from sodium benzophenone ketyl prior to use. Li(smif), Na(smif), (smif)$_2$Zn, (^{o}Mesmif)H, (^{o}Me$_2$smif)H,[5] and 1,3-(2-pyridyl)-2-azapropene ((smif)H),[25] were prepared according to literature procedures. Lithium bis(trimethylsilyl)amide was purchased from Aldrich and recrystallized from hexanes prior to use. All other chemicals were commercially available and used as received.

NMR spectra were obtained using INOVA 400 and 500 MHz spectrometers. Chemical shifts are reported relative to benzene-d_6 (^{1}H δ 7.16; ^{13}C{^{1}H} δ 128.39), toluene-d_8 (^{1}H δ 2.09; ^{13}C{^{1}H} δ 20.4), and THF-d_8 (^{1}H δ 3.58; ^{13}C{^{1}H} δ 67.57). Multidimensional techniques were conducted using INOVA software affiliated with the spectrometers. Solution magnetic measurements were conducted via Evans' method in toluene-d_8.[66] Elemental analyses were performed by Robertson Microlit Laboratories, Madison, New Jersey, and at the University of Erlangen-Nuremberg, Erlangen, Germany.

5.2. Procedures. *5.2.1. (smif)Fe{N(SiMe$_3$)$_2$} (**1**) and [{(Me$_3$Si)$_2$N}-Fe]$_2$(μ-κ^3,κ^3-N,py$_2$-smif,smif) (**2**).* A solution of (smif)H (0.700 g, 3.55 mmol) in 10 mL of Et$_2$O was added dropwise to a stirring solution of Fe{N(SiMe$_3$)$_2$}$_2$(THF) (1.592 g, 3.55 mmol) in Et$_2$O (10 mL) at 23 °C. The solution immediately became dark green (**1**). The reaction was degassed and allowed to stir at 23 °C for 3 h, and volatiles were

dx.doi.org/10.1021/ic302783y | Inorg. Chem. 2013, 52, 3295−3312

removed. The orange crystalline solid was triturated with pentane, stripped, and filtered in Et_2O to produce 1.090 g of **2** (74%). ^1H NMR (THF-d_8, 400 MHz): δ −0.01 ($\nu_{1/2} \approx 9$ Hz, 1H), 34.57 ($\nu_{1/2} \approx 380$ Hz, 9H), 46.70 ($\nu_{1/2} \approx 35$ Hz, 1H), 46.99 ($\nu_{1/2} \approx 110$ Hz, 1H), 86.21 ($\nu_{1/2} \approx 790$ Hz, 1H), 165.40 ($\nu_{1/2} \approx 620$ Hz, 1H). ^1H NMR (C_6D_6, 400 MHz): δ −14.34 ($\nu_{1/2} \approx 270$ Hz, 9H), −10.83 ($\nu_{1/2} \approx 100$ Hz, 1H), 71.49 ($\nu_{1/2} \approx 130$ Hz, 1H), 79.24 ($\nu_{1/2} \approx 200$ Hz, 1H), 136.99 ($\nu_{1/2} \approx 500$ Hz, 1H), 203.24 ($\nu_{1/2} \approx 430$ Hz, 1H).

*5.2.2. (dpma)Fe{N(SiMe$_3$)$_2$} (**3**).*[26] To a solution of Fe{N(SiMe$_3$)$_2$}$_2$(THF) (0.500 g, 1.11 mmol) in Et_2O (10 mL) at −78 °C was added di-(2-picolyl)amine (0.222 g, 1.11 mmol) in 10 mL of Et_2O via syringe under argon. Upon warming to 23 °C, the solution became red and continued to stir for 3 h. The reaction was degassed, cooled to −78 °C, and filtered. Red needles of **3** (0.297 g, 64%) were washed with cold Et_2O. ^1H NMR (C_6D_6, 400 MHz): δ 12.73 ($\nu_{1/2} \approx 1900$ Hz, Si(CH_3)$_3$, 18 H), 25.20 ($\nu_{1/2} \approx 520$ Hz, CH_2, 2H), 36.57 ($\nu_{1/2} \approx 1200$ Hz, py-C*H*, 1H), 81.90 ($\nu_{1/2} \approx 2400$ Hz, py-C*H*, 1H), 130.74 ($\nu_{1/2} \approx 2200$ Hz, py-C*H*, 1H), 182.06 ($\nu_{1/2} \approx 3100$ Hz, py-C*H*, 1H). UV−vis (benzene) = 549 nm ($\varepsilon \sim 1500$ M^{-1} cm^{-1}). Anal. Calcd for $H_{30}C_{18}N_4Si_2Fe$: C, 52.16; H, 7.30; N, 13.52. Found: C, 52.32; H, 7.32; N, 13.49. μ_{eff} (SQUID, 293 K) = 3.0 μ_B.

*5.2.3. (^{o}Mesmif)FeN(SiMe$_3$)$_2$ (**4**) and [{(Me$_3$Si)$_2$N}Fe]$_2$(μ-κ^3,κ^3-N,py$_2$-^{o}Mesmif,^{o}Mesmif) (**5**).* To a stirring solution of Fe{N(SiMe$_3$)$_2$}$_2$(THF) (0.500 g, 1.11 mmol) in 10 mL of Et_2O was slowly added a solution of (^{o}Mesmif)H (0.235 g, 1.11 mmol) in Et_2O (8 mL) at 23 °C. The reaction mixture became emerald-teal green (**4**). The reaction was degassed, warmed to 23 °C, and stirred for 20 h while yellow-orange crystals precipitated from solution. The suspension was concentrated, and yellow-orange crystals were isolated by filtration to yield **5** (0.225, 47%). ^1H NMR (C_6D_6, 400 MHz): δ −21.82 ($\nu_{1/2} \approx 38$ Hz, C*H*, 1H), −26.10 ($\nu_{1/2} \approx 38$ Hz, C*H*, 1H), −13.23 ($\nu_{1/2} \approx 413$ Hz, CH_3, 3H), 0.75 ($\nu_{1/2} \approx 300$ Hz, Si(CH_3)$_3$, 18H), 14.26 ($\nu_{1/2} \approx 131$ Hz, py-C*H*, 1H), 40.95 ($\nu_{1/2} \approx 23$ Hz, py-C*H*, 1H), 46.13 ($\nu_{1/2} \approx 374$ Hz, py-C*H*, 1H), 47.74 ($\nu_{1/2} \approx 23$ Hz, py-C*H*, 1H), 59.84 ($\nu_{1/2} \approx 96$ Hz, py-C*H*, 1H), 64.39 ($\nu_{1/2} \approx 96$ Hz, py-C*H*, 1H), 252.29 ($\nu_{1/2} \approx 1000$ Hz, py-C*H*, 1H).

*5.2.4. [{(Me$_3$Si)$_2$N}Fe]$_2$(μ:κ^3-N,py,py′,κ^3-N′,py′,-py-^{o}Me$_2$smif-^{o}Me$_2$smif) (**6**).* In a N_2 drybox, a 5 mL scintillation vial was charged with 50 mg of Fe[N(TMS)$_2$]$_2$(THF) (0.11 mmol) and 0.5 mL of Et_2O. A solution of ^{o}Me$_2$smifH (25 mg, 0.11 mmol) in Et_2O (1.0 mL) was added dropwise at room temperature while stirring. Upon addition, the solution changed from the light green characteristic of Fe[N(TMS)$_2$]$_2$(THF) to a darker pine green. The reaction mixture was allowed to stir an additional 20 min, and solvent was removed *in vacuo* to yield a dark green powder. Evidence of highly colored (^{o}Me$_2$smif)$_2$Fe (teal solution, dark teal/gold in solid state) was noted >12 h in solution and after 2−3 days in the solid state. Crystalline [(^{o}Me$_2$Smif)FeN(TMS)$_2$]$_2$ (32 mg, 33%) was isolated from a saturated pentane solution at −30 °C after 3 days. ^1H NMR (C_6D_6, 400 MHz): δ −13.11 ($\nu_{1/2} \approx 65$ Hz, py-C*H*, 4H), −1.47 ($\nu_{1/2} \approx 600$ Hz, CH_3, 6H), 3.72 ($\nu_{1/2} = 50$ Hz, im-C*H*, 2H), 11.60 ($\nu_{1/2} = 382$ Hz, Si(CH_3)$_3$, 36H), 16.00 ($\nu_{1/2} = 750$ Hz, CH_3, 6Hz), 34.24 ($\nu_{1/2} = 95$ Hz, py-C*H*, 4H), 40.07 ($\nu_{1/2} = 91$ Hz, py-C*H*, 4H), 121.39 ($\nu_{1/2} = 493$ Hz, C*H*, 2H). μ_{eff} (SQUID, 300 K) = 7.26 μ_B.

5.2.5. 2,4-Di-(2-pyridyl)-3-aza-2-pentene (^{b}Me$_2$smif)H). A solution of (smif)H (1.000 g, 5.07 mmol) in 20 mL of THF was slowly added to a suspension of NaH (0.243 g, 10.13 mmol) in 15 mL of THF at 0 °C. The reaction mixture turned magenta and was stirred at 0 °C for 3 h prior to the addition of CH_3I (0.63 mL, 10.11 mmol). After stirring at 23 °C for 12 h, the solution appeared orange-red. The volatiles were removed *in vacuo*, and the residue was filtered in CH_2Cl_2. Methylene chloride was removed, and the solid was triturated with Et_2O and filtered to yield an orange solid (1.138 g, 99%). ^1H NMR (C_6D_6, 500 MHz): δ 1.67 (d, CH_3, 3H, J = 7 Hz), 2.37 (s, im-CH_3, 3H), 5.19 (q, C*H*, 1H, J = 6.5 Hz), 6.67 (t, py-C^5*H*, 1H, J = 5.5 Hz), 6.68 (t, py^{im}-C^5*H*, 1H, J = 5.5 Hz), 7.17 (t, py-C^4*H*, 1H, J = 7.5 Hz), 7.19 (t, py^{im}-C^4*H*, 1H, J = 7.5 Hz), 7.63 (d, py-C^3*H*, 1H, J = 8 Hz), 8.39 (d, py^{im}-C^3*H*, 1H, J = 8 Hz), 8.44 (d, py-C^6*H*, 1H, J = 3.5 Hz), 8.54 (d, py^{im}-C^6*H*, 1H, J = 4 Hz). $^{13}C\{^1H\}$ NMR (C_6D_6, 125 MHz): δ 13.97 (CH_3), 23.52 (im-CH_3), 62.94 (im-CH), 121.37 (py-C^{3}H), 121.49 (py^{im}-C^{3}H), 122.05 (py-C^{5}H), 124.38 (py^{im}-C^{5}H), 136.08 (py-C^{4}H), 136.50 (py^{im}-C^{4}H), 148.81 (py-C^{6}H), 149.66 (py^{im}-C^{6}H), 158.60 (im-CH), 165.95 (py^{im}-C^2), 166.23 (py-C^2).

*5.2.6. (^{b}Me$_2$smif)$_2$Fe (**7**).* To a 50 mL round-bottom flask charged with Fe{N(SiMe$_3$)$_2$}$_2$(THF) (0.996 g, 2.22 mmol) and (^{b}Me$_2$smif)H (1.000 g, 4.44 mmol) was vacuum transferred 25 mL of THF at −78 °C. The reaction mixture became dark green and was stirred at 23 °C for 2 d. The volatiles were removed *in vacuo*. The solid was first triturated with pentane (2 × 15 mL) and then Et_2O prior to filtering and washing with cold Et_2O to yield a mossy green solid (0.802 g, 72%). ^1H NMR (C_6D_6, 400 MHz): δ 2.54 (s, CH_3, 3H), 5.87 (t, py-C^4*H*, 1H, J = 8 Hz), 6.03 (d, py-C^3*H*, 1H, J = 8.4 Hz), 6.49 (t, py-C^5*H*, 1H, J = 4 Hz), 7.80 (d, py-C^6*H*, 1H, J = 5.2 Hz). $^{13}C\{^1H\}$ NMR (C_6D_6, 100 MHz): δ 17.55 (CH_3), 111.83 (CCH_3), 115.80 (py-C^{5}H), 119.79 (py-C^{3}H), 134.70 (py-C^{4}H), 152.12 (py-C^{6}H), 165.98 (py-C^2).

*5.2.7. (^{b}Me$_2$^{o}Me$_2$smif)FeN(SiMe$_3$)$_2$ (**8**) and [{(Me$_3$Si)$_2$N}Fe]$_2$(μ-κ^4,κ^4-N,py$_2$,C-(^{b}Me,^{b}CH$_2$,^{o}Me$_2$(smif) H))$_2$ (**9**).* A small tube fitted to a 180° needle valve was charged with Fe{N(SiMe$_3$)$_2$}$_2$(THF) (0.105 g, 0.23 mmol) and (^{b}Me$_2$smif)H (0.025 g, 0.30 mmol). A bell pepper green solution appeared immediately upon addition of benzene. The reaction was degassed, sealed under vacuum, and allowed to sit for 2 days at 23 °C. The tube was opened, and benzene was decanted. Red-orange crystals of **9** were washed with Et_2O. (0.069 g, 63%). ^1H NMR (**8**, C_6D_6, 400 MHz): δ −50.62 ($\nu_{1/2} \approx 370$ Hz, CH_3, 3H), 18.23 ($\nu_{1/2} \approx 600$ Hz, Si(CH_3)$_3$, 9H), 21.94 ($\nu_{1/2} \approx 350$ Hz, py-C*H*, 1H), 48.25 ($\nu_{1/2} \approx 44$ Hz, py-C*H*, 1H), 57.31 ($\nu_{1/2} \approx 310$ Hz, py-C*H*, 1H), 69.57 ($\nu_{1/2} \approx 440$ Hz, CH_3, 3H). Anal. Calcd for $H_{22}C_{36}N_4Si_2Fe$: C, 56.39; H, 7.74; N, 11.96. Found: C, 56.62; H, 7.84; N, 12.04. μ_{eff} (SQUID, 293K) = 4.3 μ_B.

*5.2.8. {2,5-Di(pyrindin-2-yl)-3,4-di-(p-tolyl-2,5-dihydropyrrol-1-ide)}$_2$Fe (**11**).* To a small glass bomb reactor charged with [{(Me$_3$Si)$_2$N}Fe]$_2$(μ-κ^3,κ^3-N,py$_2$-smif,smif) (**2**, 0.600 g, 0.73 mmol) and di(*p*-tolyl)acetylene (0.300 g, 1.45 mmol) was added 12 mL of benzene, generating a dark emerald green solution ((smif)FeN(TMS)$_2$ (**1**)) that was degassed. The bomb was placed in a 50 °C oil bath for 3 days. Volatiles were removed *in vacuo*. Any unreacted **1** was washed away in pentane. The filter cake was washed with Et_2O, and the filtrates were concentrated. Cooling the solution to −78 °C yielded red crystals (0.175 g, 19%) of **11** that were filtered, and washed with cold Et_2O. ^1H NMR (C_6D_6, 400 MHz): δ 7.97 ($\nu_{1/2} \approx 105$ Hz, Si(CH_3)$_3$, 9H), 17.59 ($\nu_{1/2} \approx 40$ Hz, py-C*H*/ArC*H*, 1H), 27.39 ($\nu_{1/2} \approx 230$ Hz, CH_3, 3H), 31.89 ($\nu_{1/2} \approx 77$ Hz, py-C*H*/ArC*H*, 1H), 35.96 ($\nu_{1/2} \approx 52$ Hz, py-C*H*/ArC*H*, 1H), 98.84 ($\nu_{1/2} \approx 1100$ Hz, py-C*H*/ArC*H*, 1H), 194.18 ($\nu_{1/2} \approx 1100$ Hz, py-C*H*/ArC*H*, 1H). Anal. Calcd for $H_{84}C_{68}N_8Si_4Fe_2$: C, 66.00; H, 6.84; N, 9.05. Found: C, 67.40; H, 6.45; N, 7.59. μ_{eff} (SQUID, 293 K) = 5.3 μ_B.

5.2.9. Na(^{t}BuNCO-smif). To a solution of Na(smif) (0.300 g, 1.37 mmol) in 20 mL of THF was added *tert*-butylisocyanate (156 μL, 1.37 mmol) via syringe at −78 °C under argon. The solution was warmed to 23 °C and turned red. Volatiles were removed *in vacuo* after 2 h, and the resulting film was triturated with Et_2O to remove residual THF. Na(^{t}BuNCO-smif) was isolated as a metallic green solid (0.396 g, 91%). ^1H NMR (C_6D_6, 500 MHz): δ 1.39 (s, C(CH_3)$_3$, 9H), 6.33 (t, py-C^5*H*, 1H, J = 5.8 Hz), 6.43 (t, py′-C^5*H*, 1H, J = 5.8 Hz), 6.55 (d, py-C^3*H*, 1H, J = 8.1 Hz), 6.94 (t, py-C^4*H*, 1H, J = 7.0 Hz), 7.17 (t, py′-C^4*H*, 1H, J = 7.7 Hz), 7.81 (d, py′-C^3*H*, 1H, J = 8.1 Hz), 8.18 (s, N*H*, 1H), 8.20 (d, py-C^6*H*, 1H, J = 5.4 Hz), 8.44 (d, py′-C^6*H*, 1H, J = 3.9 Hz), 10.58 (s, C*H*, 1H). $^{13}C\{^1H\}$ NMR (C_6D_6, 125 MHz): δ 30.58 (C(CH_3)$_3$), 50.26 (C(CH_3)$_3$), 111.02 (py′-C^{3}H), 116.24 (py′-C^{5}H), 116.94 (py-C^{3}H), 118.74 (py-C^{5}H), 121.24 (C(C═O)), 123.58 (CH), 135.18 (py-C^{4}H), 136.52 (py′-C^{4}H), 148.28 (py-C^{6}H), 150.40 (py′-C^{6}H), 157.79 (C═O), 160.47 (py′-C^2), 169.93 (py-C^2).

*5.2.10. (^{t}BuNCO-smif)$_2$Fe (**14a**).* a. To a small glass bomb reactor charged with (smif)$_2$Fe (**13**) (0.150 g, 0.33 mmol) was added 10 mL of C_6H_6. The bomb was cooled to −78 °C, and *tert*-butylisocyanate (76 μL, 0.66 mmol) was added via GC syringe under argon. The reaction was degassed and slowly warmed to 23 °C. The solution turned deep red-orange after stirring at 23 °C for 18 h. The reaction was stirred at 23 °C for 10 days. Volatiles were removed *in vacuo*, and the reaction mixture was triturated with pentane (3 × 5 mL). After

dx.doi.org/10.1021/ic302783y | *Inorg. Chem.* 2013, 52, 3295−3312

filtering and washing with pentane, **14a** was isolated as a dark red solid (0.102 g, 47%). **b**. To a 25 mL round-bottom flask charged with $FeBr_2(THF)_2$ (0.141 g, 0.39 mmol) and Na(^{t}BuNCO-smif) (0.250 g, 0.79 mmol) was vacuum transferred 20 mL of THF at −78 °C. The solution turned red-orange upon warming to 23 °C and was stirred for 18 h. Volatiles were removed *in vacuo*, and the resulting solid was triturated with Et_2O prior to filtering in toluene. A dark red microcrystalline solid, **14a**, was obtained (0.154 g, 61%). ^{1}H NMR (C_6D_6, 500 MHz): δ 1.53 (s, C(CH_3)$_3$, 9H), 5.37 (s, N*H*, 1H), 5.71 (t, py-C^5*H*, 1H, J = 6.2 Hz), 5.76 (t, py′-C^5*H*, 1H, J = 6.3 Hz), 6.32 (t, py-C^4*H*, 1H, J = 7.3 Hz), 6.36 (d, py-C^3*H*, 1H, J = 7.9 Hz), 6.48 (t, py′-C^4*H*, 1H, J = 6.3 Hz), 7.03 (d, py′-C^3*H*, 1H, J = 8.5 Hz), 7.75 (d, py-C^6*H*, 1H, J = 5.3 Hz), 7.98 (d, py′-C^6*H*, 1H, J = 5.1 Hz), 9.91 (s, C*H*, 1H). ^{13}C{^{1}H} NMR (C_6D_6, 125 MHz): δ 30.08 (C(CH_3)$_3$), 51.35 (*C*(CH_3)$_3$), 113.33 (py′-C^{3}H), 116.31 (py′-C^{5}H), 116.79 (py-C^{3}H), 119.27 (py-C^{5}H), 119.95 (*C*(C═O)), 130.04 (*C*H), 135.01 (py-C^{4}H), 135.42 (py′-C^{4}H), 151.70 (py-C^{6}H), 152.06 (py′-C^{6}H), 164.40 (py′-C^2), 164.47 (*C*═O), 165.62 (py-C^2). UV−vis (benzene) = 383 nm (ε ∼ 28 000 M^{-1} cm^{-1}), 431 nm (ε ∼ 42 000 M^{-1} cm^{-1}), 534 nm (ε ∼ 19 000 M^{-1} cm^{-1}), 644 nm (ε ∼ 6000 M^{-1} cm^{-1}). Anal. Calcd for $H_{38}C_{34}N_8O_2Fe$: C, 63.16; H, 5.92; N, 17.33. Found: C, 63.24; H, 5.48; N, 16.01.

*5.2.11. (2,6-^{i}Pr$_2$-C$_6$H$_3$-NCO-smif)$_2$Fe (**14b**).* To a 25 mL round-bottom flask charged with (smif)$_2$Fe (**13**) (0.500 g, 1.12 mmol) was added 20 mL of C_6H_6. The flask was cooled to −78 °C, and 2,6-diisopropylphenylisocyanate (0.48 mL, 2.24 mmol) was added via syringe under argon. The reaction was degassed and slowly warmed to 23 °C as the solution turned deep red-orange. The reaction stirred at 23 °C for 17 h. Volatiles were removed *in vacuo*, and the reaction mixture was triturated with pentane (3 × 5 mL). After filtering and washing with pentane, **14b** was isolated as a dark red solid (0.719 g, 75%). ^{1}H NMR (C_6D_6, 400 MHz): δ 1.38 (s, CH(CH_3)$_2$, 12H), 3.56 (sept, C*H*(CH_3)$_2$, 2H, J = 6.9 Hz), 5.84 (t, py-C^5*H*, py′-C^5*H*, 2H, J = 5.3 Hz), 6.33 (d, Ar−C^3*H*, 2H, J = 3.8 Hz), 6.54 (t, Ar-C^4*H*, 1H, J = 7.3 Hz), 6.98 (s, N*H*, 1H), 7.31 (m, py-C^3*H*, py-C^4*H*, py′-C^4*H*, 3H), 7.44 (d, py′-C^3*H*, 1H, J = 8.4 Hz), 7.77 (d, py-C^6*H*, 1H, J = 5.4 Hz), 7.99 (d, py′-C^6*H*, 1H, J = 5.2 Hz), 10.15 (s, C*H*, 1H). ^{13}C{^{1}H} NMR (C_6D_6, 100 MHz): δ 24.36 (CH(CH_3)$_2$), 24.38 (CH(*C*H_3)$_2$), 30.07 (*C*H(CH_3)$_2$), 114.11 (py′-C^{3}H), 117.00 (py′-C^{5}H), 117.98 (py-C^{3}H), 118.34 (py-C^{5}H), 119.89 (*C*(C═O)), 124.07 (*C*H), 127.92 (Ar-C^{3}H), 133.02 (Ar-C^{4}H), 134.18 (py-C^{4}H), 135.24 (py′-C^{4}H), 136.08 (Ar-C^1), 145.41 (Ar-C^2), 151.42 (py-C^{6}H), 151.88 (py′-C^{6}H), 163.97 (py′-C^2), 164.55 (*C*═O), 165.51 (py-C^2). UV−vis (benzene) = 381 nm (ε ∼ 33 000 M^{-1} cm^{-1}), 427 nm (ε ∼ 46 000 M^{-1} cm^{-1}), 525 nm (ε ∼ 21 000 M^{-1} cm^{-1}), 638 nm (ε ∼ 7000 M^{-1} cm^{-1}). Anal. Calcd for $H_{54}C_{50}N_8O_2Fe$: C, 70.25; H, 6.37; N, 13.11. Found: C, 69.86; H, 6.34; N, 13.00.

*5.2.12. (dpma)$_2$Fe (**15**).* **a**. To a solution of Fe{N(SiMe$_3$)$_2$}$_2$(THF) (0.250 g, 0.56 mmol) in Et_2O (10 mL) at −78 °C was added [(2-py)C*H*$_2$]$_2$NH (0.222 g, 1.11 mmol) in 5 mL of Et_2O via syringe under argon. The solution became dark blue after 30 min at 23 °C and was stirred for 12 h. The volatiles were removed *in vacuo*. The residue was dissolved in benzene and filtered through Celite. Addition of pentane facilitated the crystallization of **15** as dark blue-metallic purple crystals (0.188 g, 75%). ^{1}H NMR (C_6D_6, 400 MHz): δ 8.47 ($\nu_{1/2}$ ≈ 40 Hz, 1H), 41.31 ($\nu_{1/2}$ ≈ 70 Hz, 1H), 50.37 ($\nu_{1/2}$ ≈ 100 Hz, 2H), 56.60 ($\nu_{1/2}$ ≈ 180 Hz, 1H), 163.05 ($\nu_{1/2}$ ≈ 2900 Hz, 1H). Anal. Calcd for $H_{24}C_{24}N_6Fe$: C, 63.73; H, 5.35; N, 18.58. Found: C, 63.53; H, 5.05; N, 17.69. **b**. (d_4-dpma)$_2$Fe (15-d_8). To a solution of Fe{N(SiMe$_3$)$_2$}$_2$-(THF) (0.329 g, 0.73 mmol) in Et_2O (10 mL) at −78 °C was added (d_4-dpma)D (0.300 g, 1.47 mmol) in 9 mL of Et_2O via syringe under argon. The solution changed color from pale green to dark blue after 30 min at 23 °C and was stirred for 20 h. The volatiles were removed *in vacuo*. The solid was taken up and filtered in Et_2O. The filtrates were concentrated, cooled to −78 °C, and filtered, and the resulting dark blue crystals, **15**-d_8, were washed with cold Et_2O (0.220 g, 66%).

*5.2.13. (dpma)(smif)Fe (**16**).* **a**. To a stirred suspension of [{(Me$_3$Si)$_2$N}Fe]$_2$(μ-κ^3,κ^3-*N*,py$_2$-smif,smif) (**2**, 0.300 g, 0.36 mmol) in 20 mL of Et_2O at −78 °C was slowly added a solution of di-(2-picolyl)amine (0.145 g, 0.73 mmol) in Et_2O (10 mL) under argon. The suspension immediately changed from emerald green to red. The reaction was degassed and allowed to stir at 23 °C for 3 h while dark red crystals precipitated from solution. The reaction mixture was concentrated, filtered cold, and washed with cold Et_2O to yield a mixture of **16** and (smif)$_2$Fe (**13**) (16:1, 0.225 g, 63%). **b**. To a stirred solution of (dpma)FeN(TMS)$_2$ (**3**) **15-Fe** (0.300 g, 0.72 mmol) in 20 mL of Et_2O at −78 °C was slowly added a solution of (smif)H (0.143 g, 0.72 mmol) in Et_2O (10 mL) under argon. The reaction was degassed. The reaction mixture changed color from cherry red to dark blue to purple to dark red as the solution warmed to 23 °C. Dark red crystals precipitated from solution while it stirred at 23 °C for 3 h. The reaction mixture was concentrated, filtered cold, and washed with cold Et_2O to yield a mixture of **16** and **13** (2:1, 0.260 g, 51%). ^{1}H NMR (C_6D_6, 400 MHz): δ 8.70 ($\nu_{1/2}$ ≈ 19 Hz, CH_2, 2H), 14.98 ($\nu_{1/2}$ ≈ 40 Hz, py-C*H*, 1H), 16.95 ($\nu_{1/2}$ ≈ 40 Hz, py-C*H*, 1 H), 19.48 ($\nu_{1/2}$ ≈ 60 Hz, py-C*H*, 1H), 21.80 ($\nu_{1/2}$ ≈ 80 Hz, py-C*H*, 1H), 30.37 ($\nu_{1/2}$ ≈ 187 Hz, py-C*H*, 1H), 32.02 ($\nu_{1/2}$ ≈ 234 Hz, py-C*H*, 1H), 47.34 ($\nu_{1/2}$ ≈ 388 Hz, C*H*, 1H), 81.73 ($\nu_{1/2}$ ≈ 1900 Hz, py-C*H*, 1H), 183.55 ($\nu_{1/2}$ ≈ 3500 Hz, py-C*H*, 1H).

*5.2.14. (dpma)FeOCHPh$_2$ (**17**).* To a 50 mL round-bottom flask charged with **3** (0.212 g, 0.256 mmol) and diphenylmethanol (0.095 g, 0.52 mmol) was vacuum transferred 15 mL of Et_2O at −78 °C, resulting in a red solution. The solution darkened to red-purple and was stirred at 23 °C for 3 h. The solution was concentrated, filtered, and washed with cold Et_2O to yield a purple solid (0.194 g). ^{1}H NMR spectral analysis indicated **17** as the major product, but repeated syntheses showed variable amounts of impurities that could not be removed. A quench of the product with H_2O afforded a 1.06:1.00 ratio of di-(2-picolyl)amine/diphenylmethanol. ^{1}H NMR (signals attributed to **17**, C_6D_6, 400 MHz): δ 7.62 (1H, $\nu_{1/2}$ = 20 Hz), 8.33 (2H, $\nu_{1/2}$ = 27 Hz), 12.76 (2H, $\nu_{1/2}$ = 144 Hz), 13.75 (1H, $\nu_{1/2}$ = 52 Hz), 20.84 (1H, $\nu_{1/2}$ = 83 Hz), 24.32 (1H, $\nu_{1/2}$ = 61 Hz), 65.56 (1H, $\nu_{1/2}$ = 691 Hz), 135.50 (1H, $\nu_{1/2}$ = 972 Hz).

*5.2.15. (smif)FeOCHPh$_2$ (**18**).* To a 25 mL round-bottom flask charged with [{(Me$_3$Si)$_2$N}Fe]$_2$(μ-κ^3,κ^3-*N*,py$_2$-smif,smif) (**2**, 0.200 g, 0.24 mmol) and diphenylmethanol (0.089 g, 0.48 mmol) was vacuum transferred 15 mL of THF at −78 °C, resulting in an emerald green solution. After stirring at 23 °C for 2.5 days, volatiles were removed *in vacuo* from the dark kelly green solution. The solid was washed with pentane to remove excess diphenylmethanol. The ^{1}H NMR spectrum of the green, microcrystalline sample revealed a 1:1 mixture of (smif)$_2$Fe and **18**. Attempts to purify the sample were unsuccessful, but diphenylmethanol was identified from hydrolysis by ^{1}H NMR spectra analysis in C_6D_6. ^{1}H NMR (assignments tentative, C_6D_6, 400 MHz): δ −29.46 ($\nu_{1/2}$ ≈ 365 Hz, Ar-C*H*, 4H), −0.77 ($\nu_{1/2}$ ≈ 61 Hz, Ar-C*H*, 4H), 1.49 ($\nu_{1/2}$ ≈ 20 Hz, C*H*,1H), 3.40 ($\nu_{1/2}$ ≈ 38 Hz, Ar-C*H*, 2H), 3.74 ($\nu_{1/2}$ ≈ 30 Hz, C*H*, 1H), 35.55 ($\nu_{1/2}$ ≈ 47 Hz, py-C*H*, 1H), 66.47 ($\nu_{1/2}$ ≈ 73 Hz, py-C*H*, 1H), 125.50 ($\nu_{1/2}$ ≈ 861 Hz, py-C*H*, 1H), 254.92 ($\nu_{1/2}$ ≈ 554 Hz, py-C*H*, 1H).

5.2.16. (d_4-dpma)H. To a 50 mL round-bottom flask containing a solution of 2-cyanopyridine (1.658 g, 15.93 mmol) in 16 mL of CH_3OD was added sodium borodeuteride (2.000 g, 47.78 mmol). The resulting cloudy suspension was refluxed under argon for 16 h. The yellow suspension was cooled to 23 °C, filtered, and washed with CH_3OD. Volatiles were removed from the yellow filtrates *in vacuo*, yielding a yellow solid that was dissolved in 10 mL of D_2O, stirred for 1 h at 23 °C, and extracted with CH_2Cl_2 (3 × 10 mL). Organic layers were combined, dried over Na_2SO_4, and filtered, and volatiles were removed *in vacuo* to yield an orange-yellow liquid containing both (2-pyridyl)CD_2ND_2 and (d_4-dpma)D, which were separated via distillation under dynamic vacuum: (2-pyridyl)CD_2ND_2 (0.479g, 28%) and (d_4-dpma)D (0.698 g, 44%). (2-pyridyl)CD_2ND_2: ^{1}H NMR (C_6D_6, 400 MHz): δ 6.62 (dd, py-C^5*H*, 1H, J = 7.5, 4.8 Hz), 6.88 (dt, py-C^3*H*, 1H, J = 7.8, 1.2 Hz), 7.05 (td, py-C^4*H*, 1H, J = 7.7, 1.8 Hz), 8.47 (d, py-C^6*H*, 1H, J = 4.8 Hz). ^{13}C{^{1}H} NMR (C_6D_6, 100 MHz): δ 121.31 (py-C^{3}H), 121.79 (py-C^{5}H), 136.24 (py-C^{4}H), 149.77 (py-C^{6}H), 163.44 (py-C^2). (d_4-dpma)D: ^{1}H NMR (C_6D_6, 400 MHz): δ 6.62 (t, py-C^5*H*, 1H, J = 5.6 Hz), 7.08 (m, py-C^3*H*, py-C^4*H*, 2H), 8.47 (d, py-C^6*H*, 1H, J = 4.7 Hz). ^{13}C{^{1}H} NMR (C_6D_6, 100

dx.doi.org/10.1021/ic302783y | *Inorg. Chem.* 2013, 52, 3295−3312

MHz): δ 122.98 (py-C^3H), 123.32 (py-C^5H), 137.21 (py-C^4H), 150.82 (py-C^6H), 162.27 (py-C^2).

*5.2.17. [{(Me$_3$Si)$_2$N}Fe]$_2$(μ-κ^3,κ^3-N,py$_2$-smif,smif) (**2**).* An orange parallelepiped crystal (0.40 × 0.20 × 0.15 mm) of **2** was obtained from a pentane solution cooled from 80 °C. A total of 32 284 reflections were collected with 7293 determined to be symmetry-independent (R_{int} = 0.0488), and 5519 were greater than 2σ(I). A semiempirical absorption correction from equivalents was applied, and the refinement utilized $w^{-1} = \sigma^2(F_o^2) + (0.0511p)^2 + 0.0000p$, where $p = ((F_o^2 + 2F_c^2)/3)$.

*5.2.18. [{(Me$_3$Si)$_2$N}Fe]$_2$(μ:κ^3-N,py,py′,κ^3-N′,py′,-py-^{o}Me$_2$smif-^{o}Me$_2$smif) (**6**).* A green block (0.40 × 0.20 × 0.15 mm) was obtained from a benzene/pentane mixture at 23 °C. A total of 22 647 reflections were collected with 5817 determined to be symmetry-independent (R_{int} = 0.0295), and 4615 were greater than 2σ(I). A semiempirical absorption correction from equivalents was applied, and the refinement utilized $w^{-1} = \sigma^2(F_o^2) + (0.0491p)^2 + 0.8812p$, where $p = ((F_o^2 + 2F_c^2)/3)$. One SiMe$_3$ showed a slight disorder and was modeled accordingly.

*5.2.19. [{(Me$_3$Si)$_2$N}Fe]$_2$(μ-κ^4,κ^4-N,py$_2$,C-(^{b}Me,^{b}CH$_2$,^{o}Me$_2$(smif)H))$_2$ (**9**).* A red needle (0.60 × 0.10 × 0.05 mm) of **8** was obtained from a 1:1 benzene/pentane mixture at 23 °C. A total of 20 055 reflections were collected with 4095 determined to be symmetry-independent (R_{int} = 0.0609), and 3-085 were greater than 2σ(I). A semiempirical absorption correction from equivalents was applied, and the refinement utilized $w^{-1} = \sigma^2(F_o^2) + (0.0368p)^2 + 0.3358p$, where $p = ((F_o^2 + 2F_c^2)/3)$. One of the SiMe$_3$ groups was disordered and modeled accordingly.

*5.2.20. [{2,5-Di(pyrindin-2-yl)-3,4-di-(p-tolyl-2,5-dihydropyrrol-1-ide)}FeN(SiMe$_3$)$_2$]$_2$ (**11**).* A red plate (0.60 × 0.30 × 0.05 mm) was obtained from diethyl ether at 23 °C. A total of 69 998 reflections were collected with 15 480 determined to be symmetry-independent (R_{int} = 0.0467), and 10 139 were greater than 2σ(I). A semiempirical absorption correction from equivalents was applied, and the refinement utilized $w^{-1} = \sigma^2(F_o^2) + (0.0606p)^2 + 0.0000p$, where $p = ((F_o^2 + 2F_c^2)/3)$. SQUEEZE was applied to a disordered solvent molecule.

*5.2.21. (2,6-^{i}PrC$_6$H$_3$-NCO-smif)$_2$Fe (**14b**).* A dark black-red needle (0.45 × 0.10 × 0.03 mm) was obtained from a mixture of THF and pentane at 23 °C. A total of 57 325 reflections were collected with 5564 determined to be symmetry-independent (R_{int} = 0.1560), and 2984 were greater than 2σ(I). A semiempirical absorption correction from equivalents was applied, and the refinement utilized $w^{-1} = \sigma^2(F_o^2) + (0.0911p)^2 + 0.0000p$, where $p = ((F_o^2 + 2F_c^2)/3)$. SQUEEZE was applied to a disordered solvent molecule.

*5.2.22. (dpma)$_2$Fe (**15**).* A thin blue plate (0.60 × 0.15 × 0.05 mm) of **14** was obtained from 1:1 benzene/pentane at 23 °C. The crystal was determined to be a merohedral twin. A total of 37 723 reflections were collected, with 7419 determined to be symmetry-independent (R_{int} = 0.0594), and 6031 were greater than 2σ(I). A semiempirical absorption correction from equivalents was applied, and the refinement utilized $w^{-1} = \sigma^2(F_o^2) + (0.0307p)^2 + 0.4679p$, where $p = ((F_o^2 + 2F_c^2)/3)$.

5.3. Single-Crystal X-Ray Diffraction Studies. Upon isolation, the crystals were covered in polyisobutenes and placed under a 173 K N_2 stream on the goniometer head of a Siemens P4 SMART CCD area detector (graphite-monochromated MoKα radiation, λ = 0.71073 Å). The structures were solved by direct methods (SHELXS). All non-hydrogen atoms were refined anisotropically unless stated, and hydrogen atoms were treated as idealized contributions (Riding model). Any deviation from this protocol will be noted for the individual descriptions below.

5.4. Equilibrium Study: 2 (smif)FeN(SiMe$_3$)$_2$ (1) ⇄ [(TMS)$_2$-NFe]$_2$(smif)$_2$ (2). A series of five NMR tubes were charged with known concentrations of (smif)FeN(SiMe$_3$)$_2$ (**1**). The solutions (3.4 × 10^{-3} to 2.4 × 10^{-2} M) of **2** in THF-d_8 were prepared in a 5 mL volumetric flask, and ^{1}H NMR spectra were obtained at ambient temperature (~23 °C). The chemical shift associated with the smif "backbone" CH was monitored as it exhibited the largest change as concentrations varied. The equilibrium constant, ~ 4 × 10^{-4} M^{-1}, was fit using the least-squares method developed for determining the NMR monomer shift and equilibrium constant for self-associating systems.[22]

5.5. Hydrogenation and Deuteration Studies. Flame-dried NMR tubes, sealed to 14/20 ground glass joints, were charged with (dpma)$_2$Fe **15** (0.015 g, 0.033 mmol), 2 equiv (0.066 mmol) of the appropriate organic substrate, and 0.5 mL of C_6D_6. The tube was fitted with a 180° needle valve and freeze−pump−thaw degassed three times before sealing. Reaction progress was monitored via ^{1}H NMR spectroscopy. Deuteration studies were performed in flame-dried J-Young NMR tubes. Several deuteration experiments were performed in flame-dried and silylated J-Young tubes. Results are summarized in Scheme 3 and listed in the Supporting Information.

5.6. Cyclotrimerization Studies. Flame-dried NMR tubes, sealed to 14/20 ground glass joints, were charged with 0.5 mL solutions of known concentrations of an iron compound in the glovebox. The tubes were attached to a calibrated gas bulb and degassed on the vacuum line via freeze−pump−thaw cycle. After condensing 2-butyne at 77 K, the tubes were sealed with a torch. Reaction progress was monitored via ^{1}H NMR spectroscopy by observing the disappearance of 2-butyne (δ 1.50 ppm) and appearance of hexamethylbenzene (δ 2.13 ppm). Upon completion, the tube was opened in the glovebox and the contents were transferred into a J Young tube containing 0.010 g of ferrocene. A ^{1}H NMR spectrum was obtained, and integrations permitted quantification of hexamethylbenzene produced, turnover number, and turnover frequency. The C_6D_6 stock solutions (4.5 × 10^{-3} to 1.3 × 10^{-2} M for {Fe{N(TMS)$_2$}$_2$(THF) and 4.8 × 10^{-3} to 1.5 × 10^{-2} M for **1**) were prepared using 2 or 5 mL volumetric flasks.

5.7. Magnetic Susceptibility Measurements. Magnetic susceptibility measurements of crystalline powdered samples (10−30 mg) were performed on a Quantum Design MPMS-5 SQUID magnetometer at 10 kOe (1 T) between 5 and 300 K for all samples. All sample preparations and manipulations were performed under an inert atmosphere due to the air sensitivity of the samples. The samples were measured in gelatin capsules, and the diamagnetic contribution from the sample container was subtracted from the experimental data. Pascal's constants[67] were used to subtract diamagnetic contributions, yielding paramagnetic susceptibilities. The program julX written by E. Bill was used for (elements of) the simulation and analysis of magnetic susceptibiltiy data.[68]

5.8. Mössbauer Spectroscopy. ^{57}Fe Mössbauer spectra were recorded on a WissEl Mössbauer spectrometer (MRG-500) at 77 K in constant acceleration mode. ^{57}Co/Rh was used as the radiation source. WinNormos for Igor Pro software has been used for the quantitative evaluation of the spectral parameters (least-squares fitting to Lorentzian peaks). The minimum experimental line widths were 0.20 mms^{-1}. The temperature of the samples was controlled by an MBBC-HE0106 MÖSSBAUER He/N_2 cryostat within an accuracy of ±0.3 K. Isomer shifts were determined relative to α-iron at 298 K.

5.9. Computational Methods. B3LYP[69−73] geometry optimization utilized the Gaussian03 suite of programs; the 6-31G(d) basis set was employed. Tests with the larger 6-311+G(d) basis set did not reveal significant differences in the optimized geometries. No symmetry constraints were employed in geometry optimization. Geometry optimizations were started from both a pseudo-C_{2v} structure. Calculation of the energy Hessian was performed to confirm species as minima on their respective potential energy surfaces at this level of theory.

■ ASSOCIATED CONTENT

Ⓢ Supporting Information

Hydrogen-transfer studies from (dpma)$_2$Fe (**15**) and magnetism studies and fits for **2**, **3**, **9**, **11**, and **15**. CIF files for **6**, **9**, **11**, and **14b**.This material is available free of charge via the Internet at http://pubs.acs.org. CIF files for **2** and **15** are available via ref 4.

dx.doi.org/10.1021/ic302783y | Inorg. Chem. 2013, 52, 3295−3312

AUTHOR INFORMATION

Corresponding Author

*Fax: 607 255 4173. E-mail: ptw2@cornell.edu.

Present Address

[‖]Department of Chemistry, Purdue University, West Lafayette, Indiana 47907, United States.

Notes

The authors declare no competing financial interest.

ACKNOWLEDGMENTS

P.T.W. thanks the NSF (CHE-0718030) and Cornell University for financial support, the University of Erlangen-Nuremberg for facilities usage, especially Dr. Joerg Sutter for Mössbauer studies, and Prof. Barry K. Carpenter of Cardiff University for helpful discussions and supporting computations. T.R.C. acknowledges the NSF (CHE-1057758) for financial support.

REFERENCES

(1) Frazier, B. A.; Wolczanski, P. T.; Lobkovsky, E. B. *Inorg. Chem.* **2009**, *48*, 11576−11585.

(2) Volpe, E. C.; Wolczanski, P. T.; Lobkovsky, E. B. *Organometallics* **2010**, *29*, 364−377.

(3) Volpe, E. C.; Manke, D. R.; Bartholomew, E. R.; Wolczanski, P. T.; Lobkovsky, E. B. *Organometallics* **2010**, *29*, 6642−6652.

(4) Frazier, B. A.; Wolczanski, P. T.; Lobkovsky, E. B.; Cundari, T. R. *J. Am. Chem. Soc.* **2009**, *131*, 3428−3429.

(5) Frazier, B. A.; Bartholomew, E. R.; Wolczanski, P. T.; DeBeer, S.; Santiago-Berrios, M.; Abruña, H. D.; Lobkovsky, E. B.; Bart, S. C.; Mossin, S.; Meyer, K.; Cundari, T. R. *Inorg. Chem.* **2011**, *50*, 12414−12436.

(6) Hachmann, J.; Frazier, B. A.; Wolczanski, P. T.; Chan, G. K.-L. *ChemPhysChem.* **2011**, *12*, 3236−3244.

(7) Frazier, B. A.; Wolczanski, P. T.; Keresztes, I.; DeBeer, S.; Lobkovsky, E. B.; Pierpont, A. W.; Cundari, T. R. *Inorg. Chem.* **2012**, *51*, 8177−8186.

(8) Elliott B. Hulley, E. B; Wolczanski, P. T.; Lobkovsky, E. B. *J. Am. Chem. Soc.* **2011**, *133*, 18058−18061.

(9) Floriani, C.; Solari, E.; Franceschi, F.; Scopelliti, R.; Belanzoni, P.; Rosi, M. *Chem.—Eur. J.* **2001**, *7*, 3052−3061.

(10) Gallo, E.; Solari, E.; Re, N.; Floriani, C.; Chiesi-Villa, A.; Rizzoli, C. *J. Am. Chem. Soc.* **1997**, *119*, 5144−5154.

(11) Franceschi, F.; Hesschenbrouk, J.; Solari, E.; Floriani, C.; Re, N.; Chiesi-Villa, A.; Rizzoli, C. *J. Chem. Soc., Dalton Trans.* **2000**, 593−604.

(12) De Angelis, S.; Solari, E.; Gallo, E.; Floriani, C.; Chiesi-Villa, A.; Rizzoli, C. *Inorg. Chem.* **1996**, *35*, 5995−6003.

(13) Franceschi, F.; Solari, E.; Scopelliti, R.; Floriani, C. *Angew. Chem., Int. Ed.* **2000**, *39*, 1685−1689.

(14) (a) Franceschi, F.; Solari, E.; Floriani, C.; Chiesi-Villa, A.; Rizzoli, C.; Rosi, M. *Chem.—Eur. J.* **1999**, *5*, 708−721. (b) Rosi, M.; Sgamellotti, A.; Franceschi, F.; Floriani, C. *Chem.—Eur. J.* **1999**, *5*, 2914−2920.

(15) Solari, E.; Maltese, C.; Franceschi, F.; Floriani, C.; Chiesi-Villa, A.; Rizzoli, C. *J. Chem. Soc., Dalton Trans.* **1997**, 2903−2910.

(16) Solari, E.; Maltese, C.; Latronico, M.; Floriani, C.; Chiesi-Villa, A.; Rizzoli, C. *J. Chem. Soc., Dalton Trans.* **1998**, 2395−2400.

(17) Bachmann, J.; Nocera, D. G. *J. Am. Chem. Soc.* **2005**, *127*, 4730−4743.

(18) Bachmann, J.; Nocera, D. G. *J. Am. Chem. Soc.* **2004**, *126*, 2829−2837.

(19) Venkatesan, K.; Blacque, O.; Fox, T.; Alfonso, M.; Schmalle, H. W.; Kheradmandan, S.; Berke, H. *Organometallics* **2005**, *24*, 920−932.

(20) Venkatesan, K.; Blacque, O.; Berke, H. *Organometallics* **2006**, *25*, 5190−5200.

(21) (a) Olmstead, M. M.; Power, P. P.; Shoner, S. C. *Inorg. Chem.* **1991**, *30*, 2547−2551. (b) Andersen, R. A.; Faegri, K.; Green, J. C.; Haaland, A.; Lappert, M. F.; Leung, W. P.; Rypdal, K. *Inorg. Chem.* **1988**, *27*, 1782−1786.

(22) Tan, H. K.S. *J. Chem. Soc., Faraday Trans.* **1994**, *90*, 3521−3525.

(23) Parish, R. V. *NMR, NQR, EPR, and Mössbauer Spectroscopy in Inorganic Chemistry*; Ellis Horwood: West Sussex, England, 1990.

(24) J. G. Stevens, J. G. *Hyperfine Interact.* **1983**, *13*, 221−236.

(25) Incarvito, C.; Lam, M.; Rhatigan, B.; Rheingold, A. L.; Qin, C. J.; Gavrilova, L.; Bosnich, B. *J. Chem. Soc., Dalton Trans.* **2001**, 3478−3488.

(26) Malassa, A.; Agthe, C.; Görls, H.; Friedrich, M.; Westerhausen, M. *J. Organomet. Chem.* **2010**, *695*, 1641−1650.

(27) Lu, C. C.; Bill, E.; Weyhermüller, T.; Bothe, E.; Wieghardt, K. *J. Am. Chem. Soc.* **2008**, *130*, 3181−3197.

(28) Bart, S. C.; Chlopek, K.; Bill, E.; Bouwkamp, M. W.; Lobkovsky, E.; Neese, F.; Wieghardt, K.; Chirik, P. J. *J. Am. Chem. Soc.* **2006**, *128*, 13901−13912.

(29) Wile, B. M.; Trovitch, R. J.; Bart, S. C.; Tondreau, A. M.; Lobkovsky, E. B.; Milsmann, C.; Bill, E.; Wieghardt, K.; Chirik, P. J. *Inorg. Chem.* **2009**, *48*, 4190−4200.

(30) Bart, S. C.; Lobkovsky, E.; Bill, E.; Wieghardt, K.; Chirik, P. C. *Inorg. Chem.* **2007**, *46*, 7055−7063.

(31) Wile, B. M.; Trovitch, R. J.; Bart, S. C.; Tondreau, A. M.; Lobkovsky, E. B.; Milsmann, C.; Bill, E.; Wieghardt, K.; Chirik, P. J. *Inorg. Chem.* **2009**, *48*, 4190−4200.

(32) Tondreau, A. M.; Darmon, J. D.; Wile, B. M.; Floyd, S. K.; Lobkovsky, E. B.; Chirik, P. J. *Organometallics* **2009**, *28*, 3928−3940.

(33) Volpe, E. C.; Wolczanski, P. T.; Darmon, J. M.; Lobkovsky, E. B. *Polyhedron* **2012**, *31*, in press.

(34) Sydora, O. L.; Kuiper, D. S.; Wolczanski, P. T.; Lobkovsky, E. B.; Dinescu, A.; Cundari, T. R. *Inorg. Chem.* **2006**, *45*, 2008−2021.

(35) Kauffmann, T. *Angew. Chem., Int. Ed. Engl.* **1974**, *13*, 627−638.

(36) (a) Kauffmann, T.; Ahlers, H.; Echsler, K.-J.; Schulz, H.; Tiljard, H.-J. *Chem. Ber.* **1985**, *118*, 4496−4506. (b) Kauffmann, T.; Busch, A.; Habersaat, K.; Koppelmann, E. *Chem. Ber.* **1983**, *116*, 492−499. (c) Kauffmann, T.; Koch, U.; Steinseifer, F.; Vahrenhorst, A. *Tetrahedron Lett.* **1977**, *38*, 3341−3344. (d) Kauffmann, T.; Eidenschink, R. *Chem. Ber.* **1977**, *110*, 651−655. (e) Kauffmann, T.; Eidenschink, R. *Chem. Ber.* **1977**, *110*, 645−650. (f) Kauffmann, T.; Habersaat, K.; Koppelmann, E. *Chem. Ber.* **1977**, *110*, 638−644. (g) Kauffmann, T.; Ahlers, H.; Hamsen, A.; Schulz, H.; Tilhard, H.-J.; Vahren, A. *Angew. Chem.* **1977**, *89*, 107−108.

(37) (a) Pearson, W. H.; Szura, D. P.; Postich, M. J. *J. Am. Chem. Soc.* **1992**, *114*, 1329−1345. (b) Pearson, W. H.; Mans, D. M.; Kampf, J. W. *J. Org. Chem.* **2004**, *69*, 1235−1247. (c) Pearson, W. H.; Stoy, P. *Synlett* **2003**, *7*, 903−921.

(38) Mayr, H.; Heigl, U. W.; Baran, J. *Chem. Ber.* **1993**, *126*, 1913−1916.

(39) Ciszek, J. W.; Keane, Z. K.; Cheng, L.; Stewart, M. P.; Yu, L. H.; Natelson, D.; Tour, J. M. *J. Am. Chem. Soc.* **2006**, *128*, 3179−3189.

(40) Dominguez, G.; Perez-Castells, J. *Chem. Soc. Rev.* **2011**, *40*, 3430−3444.

(41) Galan, B. R.; Rovis, T. *Angew. Chem., Int. Ed.* **2009**, *48*, 2830−2834.

(42) Gandon, V.; Aubert, C.; Malacria, M. *Chem. Commun.* **2006**, 2209−2217.

(43) Agenet, N.; Gandon, V.; Vollhardt, K. P. C.; Malacria, M.; Aubert, C. *J. Am. Chem. Soc.* **2007**, *129*, 8860−8871.

(44) Boñaga, L. V. R.; Zhang, H.-C.; Moretto, A. F.; Ye, H.; Gauthier, D. A.; Li, J.; Leo, G. C.; Maryanoff, B. E. *J. Am. Chem. Soc.* **2005**, *127*, 3473−3485.

(45) Hilt, G.; Vogler, T.; Hess, W.; Galbiati, F. *Chem. Commun.* **2005**, 1474−1475.

(46) Ferré, K.; Toupet, L.; Guerchais, V. *Organometallics* **2002**, *21*, 2578−2580.

(47) Ren, S.; Qiu, Z.; Xie, Z. *J. Am. Chem. Soc.* **2012**, *134*, 3242−3254.

(48) Bu, X. L.; Zhang, Z. X.; Zhou, X. G. *Organometallics* **2010**, *29*, 3530−3534.

(49) Basak, A. K.; Martell, A. E. *Inorg. Chem.* **1986**, *25*, 1182−1190.

(50) Spandl, J.; Kusserow, M.; Brüdgam, I. *Z. Anorg. Allg. Chem.* **2003**, *629*, 968−974.
(51) Higham, L. T.; Konno, K.; Scott, J. L.; Strauss, C. R.; Yamaguchi, T. *Green Chem.* **2007**, *9*, 80−84.
(52) Han, C.-C.; Balakumar, R.; Thirumalai, D.; Chung, M.-T. *Org. Biomol. Chem.* **2006**, *4*, 3511−3516.
(53) Abe, M.; Ye, J.; Mishima, M. *Chem. Soc. Rev.* **2012**, *41*, 3808−3820.
(54) Kamada, K.; Ohta, K.; Shimizu, A.; Kubo, T.; Kishi, R.; Takahashi, H.; Botek, E.; Champagne, B.; Nakano, M. *J. Phys. Chem. Lett.* **2010**, *1*, 937−940.
(55) Ichino, T.; Villano, S. M.; Gianola, A. J.; Goebbert, D. J.; Velarde, L.; Sanov, A.; Blanksby, S. J.; Zhou, X.; Hrovat, D. A.; Borden, W. T.; Lineberger, W. C. *Angew. Chem., Int. Ed.* **2009**, *48*, 8509−8511.
(56) Bendikov, M.; Duong, H. M.; Starkey, K.; Houk, K. N.; Carter, E. A.; Wudl, F. *J. Am. Chem. Soc.* **2004**, *126*, 7416−7417.
(57) Grapperhaus, C. A.; Kozlowski, P. M.; Kumar, D.; Frye, H. N.; Venna, K. B.; Poturovic, S. *Angew. Chem., Int. Ed.* **2007**, *46*, 4085−4088.
(58) Scheschkewitz, D.; Amii, H.; Gornitzka, H.; Schoeller, W. W.; Bourissou, D.; Bertrand, G. *Science* **2002**, *295*, 1880−1881.
(59) Trepanier, S. J.; Wang, S. *Can. J. Chem.* **1996**, *74*, 2032−2040.
(60) Barbour, J. B.; Karty, J. M. *J. Org. Chem.* **2004**, *67*, 648−654.
(61) Mo, Y.; Lin, Z.; Wu, W.; Zhang, Q. *J. Phys. Chem.* **1996**, *100*, 6469−6474.
(62) Mo, Y.; Peyerimhoff, S. D. *J. Chem. Phys.* **1998**, *109*, 1687−1697.
(63) Gobbi, A.; Frenking, G. *J. Am. Chem. Soc.* **1994**, *116*, 9275−9286.
(64) Dewar, M. J. S.; Nelson, D. J. *J. Org. Chem.* **1982**, *47*, 2614−2618.
(65) Salem, L.; Rowland, C. *Angew. Chem., Int. Ed.* **1972**, *11*, 92−111.
(66) (a) Evans, D. F. *J. Chem. Soc.* **1959**, 2003−2005. (b) Schubert, E. M. *J. Chem. Educ.* **1992**, *69*, 62.
(67) Carlin, R. L. *Magnetochemistry*; Springer-Verlag: Berlin, 1986.
(68) http://ewww.mpi-muelheim.mpg.de/bac/logins/bill/julX_en.
(69) Becke, A. D. *J. Chem. Phys.* **1993**, *98*, 5648−5652.
(70) Lee, C.; Yang, W.; Parr, R. G. *Phys. Rev. B* **1988**, *37*, 785−789.
(71) Frisch, M. J.; Trucks, G. W.; Schlegel, H. B.; Scuseria, G. E.; Robb, M. A.; Cheeseman, J. R.; Montgomery, J. A., Jr.; Vreven, T.; Kudin, K. N.; Burant, J. C.; Millam, J. M.; Iyengar, S. S.; Tomasi, J.; Barone, V.; Mennucci, B.; Cossi, M.; Scalmani, G.; Rega, N.; Petersson, G. A.; Nakatsuji, H.; Hada, M.; Ehara, M.; Toyota, K.; Fukuda, R.; Hasegawa, J.; Ishida, M.; Nakajima, T.; Honda, Y.; Kitao, O.; Nakai, H.; Klene, M.; Li, X.; Knox, J. E.; Hratchian, H. P.; Cross, J. B.; Adamo, C.; Jaramillo, J.; Gomperts, R.; Stratmann, R. E.; Yazyev, O.; Austin, A. J.; Cammi, R.; Pomelli, C.; Ochterski, J. W.; Ayala, P. Y.; Morokuma, K.; Voth, G. A.; Salvador, P.; Dannenberg, J. J.; Zakrzewski, V. G.; Dapprich, S.; Daniels, A. D.; Strain, M. C.; Farkas, O.; Malick, D. K.; Rabuck, A. D.; Raghavachari, K.; Foresman, J. B.; Ortiz, J. V.; Cui, Q.; Baboul, A. G.; Clifford, S.; Cioslowski, J.; Stefanov, B. B.; Liu, G.; Liashenko, A.; Piskorz, P.; Komaromi, I.; Martin, R. L.; Fox, D. J.; Keith, T.; Al-Laham, M. A.; Peng, C. Y.; Nanayakkara, A.; Challacombe, M.; Gill, P. M. W.; Johnson, B.; Chen, W.; Wong, M. W.; Gonzalez, C.; Pople, J. A. *Gaussian 03*, revision C.02; Gaussian, Inc.: Wallingford, CT, 2004.
(72) Nakano, H. *J. Chem. Phys.* **1993**, *99*, 7983−7992.
(73) Schmidt, M. W.; Baldridge, K. K.; Boatz, J. A.; Elbert, S. T.; Gordon, M. S.; Jensen, J. J.; Koseki, S.; Matsunaga, N.; Nguyen, K. A.; Su, S.; Windus, T. L.; Dupuis, M.; Montgomery, J. A. *J. Comput. Chem.* **1993**, *14*, 1347−1363.